A simple model simulating development and growth of an olive grove

M. Moriondo[1], L. Leolini[2], L. Brilli[1], C. Dibari[2], R. Tognetti[3], A. Giovannelli[4], B. Rapi[1], P. Battista[1], G. Caruso[5], R. Gucci[5], G. Argenti[2], A. Raschi[1], M. Centritto[4], M. Bindi[2]

[1]IBIMET-CNR, Via Madonna del Piano 10, 50019 Sesto Fiorentino (Fi), Italy

[2]University of Florence, DiSPAA, Piazzale delle Cascine 18, 50144 Firenze, Italy.

[3]Dipartimento di Agricoltura, Ambiente e Alimenti, Università degli Studi del Molise, Via Francesco De Sanctis, 86100 Campobasso, Italy.

[4]IVALSA-CNR, Via Madonna del Piano 10, 50019 Sesto Fiorentino (Fi), Italy

[5]Dipartimento di Scienze Agrarie, Alimentari e Agro-ambientali (DiSAAA-a), Università di Pisa, Via del Borghetto, 80 56124 Pisa, Italy.

Abstract

This paper describes the architecture of a simple process-based model that simulates on a daily time step growth and development of an olive agroecosystem, including the olive tree and grass cover growth and their competition for water. The model includes a phenological sub-model simulating the sequence of olive tree vegetative and reproductive stages for determining changes in biomass allocation. Final yield is calculated at the end of growing season as a fraction of total olive tree biomass accumulation. To ensure a wide applicability of the model, calibration and validation were performed across different climates, soils, planting densities and management practices. The model was firstly calibrated against daily CO_2 flux measurements obtained from an eddy covariance experimental station on a 3-year experiment, while additional sites across Tuscany region were selected to test the model effectiveness in simulating the most important plant and grass cover processes. The results pointed out that the model was able to faithfully reproduce olive tree transpiration, soil water balance total olive tree and grass cover biomass accumulation and final yield.

Keywords

Olive trees, model, process-based, eddy covariance, GPP, NPP

1. Introduction

Olive orchards are widespread agricultural systems in the Mediterranean environments (Vossen, 2007), where they play a significant role for local economies (Iraldo et al., 2013; Palese et al., 2013), and contributes to several ecosystem services (Loumou and Giourga, 2003; Fleskens et al., 2008), and climate mitigation (Brilli et al., 2013; Brilli et al., 2016; Nardino et al., 2013; Nieto et al., 2010). As such, the development of tools for reproducing olive grove dynamics is needed to provide land managers with reliable information and to evaluate system performances in response to higher temperatures (Moriondo et al., 2008; Ferrise et al., 2013; Moriondo et al., 2013; Ponti et al., 2016). Despite this, Moriondo et al. (2015) highlighted that only a few models for olive tree have been so far developed that in most cases are not readily applicable for operational purposes because of the missing simulation of plant growth limiting factors, or the high level of required parameters or because unbalanced toward specific processes. Some of these models simulate potential growth, but do not consider the impact of water stress that usually affects Mediterranean environments (Villalobos et al., 2006; Morales, 2016). Others, while considering water stress on plant growth, require specific skill or complex parametrisation to be implemented outside their calibration area. As an example, Maselli et al. (2012) simulated olive tree growth based on intercepted radiation and ground cover calculated using remotely sensed data but algorithms are not easily applicable.. The Abdel-Razik (1989) and Viola et al. (2012) models, while considering abiotic constraints, require an intense parametrisation, while the aim of the model described in Ponti et al. (2016) mainly addressed the interaction of olive fly with olive tree. In all these cases, the possible competition between olive trees and ground cover is not considered.

Building on these premises, the purpose of this paper is to describe the structure of a model simulating biomass accumulation and yield of an olive grove on a daily time step using a simplified approach accounting for the competition between ecosystem components (i.e. olive tree and grass cover) for soil water.

To ensure a wide applicability of the model, calibration and validation tests were performed in contrasting years and climates across Tuscany region. The results are discussed emphasizing the compromise between the simple structure of the model with limited data required for simulations and its effectiveness in reproducing different plant processes across a gradient of Mediterranean climates, soils and management systems (Fernández et al., 2008).

2. Materials and methods

2.1. Model description

The model simulates growth and development of the olive agroecosystem on a daily time step, which includes the simulation of olive tree and grass cover growth and their competition for water (Fig. 1). A phenological sub-model simulates the sequence of olive tree vegetative and reproductive stages for determining changes in biomass allocation. Final yield is calculated at the end of growing season as a fraction of total olive tree biomass accumulation (harvest index, HI) that may be reduced from its potential value by both heat and water stress.

2.1.1. Olive tree phenology model

Bud break and flowering phases were simulated through two modelling approaches. Building on the results in Lopez-Bernal et al. (2015) demonstrating olive tree apical buds undergo an easily-reversible endo-dormant state in winter as driven by warm temperature, the onset of bud break is simulated considering growing degree hours accumulation (GDH) above a base temperature (*tb*) from the 1st of January until a required accumulation (Eq.1).

$$GDH = \sum T_{avg\,(h)} - tb \qquad [1]$$

Where GDH is the growing degree hour accumulation above *tb* using hourly average temperature ($T_{avg(h)}$). The starts of endo-dormancy state of the buds (i.e. the stop of the growing phase) is assumed to be triggered when average daily temperatures are stably below the *tb* (SI).

Considering that flowering is dependent on both chilling and forcing temperatures for the release of endo-dormancy and eco-dormancy periods, we adopted the UniChill model proposed by Chuine (2000). The endo-dormancy period is simulated through chilling unit accumulation from September 1st until the chilling requirement (*Ccrit;* Eq. 2) while the eco-dormancy period is estimated by the forcing unit accumulation until chilling requirement is reached (*FcritFlo*; Eq. 3).

Chilling and forcing units (CU and FU) are calculated as:

$$ChillingUnits = \sum \frac{1}{1+e^{a\cdot(T_{avg}-c)^2+b\cdot(T_{avg}-c)}} \quad [2]$$

$$ForcingUnits = \sum \frac{1}{1+e^{d\cdot(T_{avg}-e)}} \quad [3]$$

Where T_{avg} is the daily average temperature, *a*, *b*, *c*, *d* and *e* being the curve shape parameters. In particular, *c* and *e* are the base temperature for chilling and forcing unit accumulation, respectively.

2.1.2. Potential dry matter accumulation

A model was developed and tested to simulate daily biomass accumulation of an olive agroecosystem, which includes the simulation of olive tree (ot) and grass cover (gr) growth and their competition for water. The key process of the model is the simulation of daily potential biomass increase (g dry matter m^{-2}) for both layers as dependent on the relevant intercepted ($Int.Rad$, rate) daily photosynthetic active radiation (Rad, MJ m^{-2}), and radiation use efficiency (RUE, g MJ^{-1}). Accordingly:

$$DM_i = Int.Rad_i \cdot Rad \cdot RUE_i \quad [4]$$

Where the sub-index *i* refer to either olive trees (*ot*) or grass (*gr*).

RUE either for olive and grass was rescaled according to a fractional value PRFT (Jones and Kiniry, 1986) calculated as:

$$PRFT_i = 1 - 0.0025 \cdot (0.25 \cdot Tmin + 0.75 \cdot Tmax - x)^2 \quad [5]$$

That accounts for the effect of sub and supra optimal temperature for grass and olive tree where optimal temperatures range from 15°C to 25°C for grass (x=18, Jones and Kiniry, 1986) and 20°C to 30°C for olive tree (x=25, Bongi et al., 1987; Carr, 2014)

$Int.Rad$ of olive tree ($Int.Rad_{OT}$) was calculated according the model proposed by Testi et al. (2006):

$$Int.Rad_{OT} = 1 - \exp(-k' \cdot v) \quad [5]$$

Where:

v is the canopy volume for unit area ($m^3\ m^{-2}$)

$$k' = 0.52 + 0.000788 * PlantD - 0.76 \cdot \exp(-1.25 * LAD) \quad [6]$$

LAD is Leaf Area Density ($m^2\ m^{-3}$) and $PlantD$ is the number of plants per hectare

At the beginning of the growing season, initial LAI of olive tree is calculated as:

$$LAI_{ini} = Vol \cdot LAD \cdot PlantA^{-1} \quad [7]$$

Where Vol (m^3) is the volume of the crown of olive tree calculated as the volume of an ellipsoid and $PlantA$ is plant spacing (i.e. inter-row×intra-row distances, m^2)

On each daily time step, the potential increase of olive tree LAI (LAI_{inc}) is calculated as the product of daily assimilated DM, a leaf partition coefficient ($PC_{lf,}$, rate) and specific leaf area (SLA, $m^2\ g^{-1}$). Accordingly:

$$LAI_{inc} = DM \cdot PC_{lf.pot} \cdot SLA \quad [8]$$

$PC_{lf\ .pot}$ changes dynamically during the season depending on phenological stage accounting for the fact that during before anthesis biomass is allocated only for vegetative biomass while after anthesis yield has highest priority for carbon allocation with respect to vegetative growth (Mariscal et al., 2000, details in section 2.2.2). The effect of alternate bearing on source/sink relationships is also accounted for by considering that in over-cropping years vegetative growth is reduced and *viceversa* (Lavee, 2007) (section 2.1.4 for details).

Cumulated LAI is then used to update the canopy volume for unit area (v) daily as used in equation 5 and calculated as:

$$v = LAI \cdot LAD^{-1} \quad [9]$$

Considering that the typical life span of olive tree leaves is two-year (Morales et al., 2016), leaves senescence is calculated as:

$$Sen_{\ leaf} = YLAI_{(y-2)}/(DOY_{end} - DOY_{ini})$$

Where YLAi is the LAI produced two years before and DOY_{end} and DOY_{ini} are the days when senescence ends and begins, assumed between DOY 365 and 1 (Morales et al., 2016).

Total dry matter cumulated from January 1st to harvest time is converted into final yield, using a fixed ratio between final yield (Y) and total dry matter (potential harvest index, HI.pot, unit less). Accordingly:

$$Y = HI.pot * \sum_{DOY=1}^{DOY=harvest\ time} DM \quad [10]$$

In unstressed conditions HI.pot has an initial value of 0.35 (Villalobos et al., 2006) that may be decreased by unfavorable meteorological events occurring at flowering and fruit set (see section 2.14 for details).

The fraction of radiation penetrating olive tree canopy (1- INT.RAD.OT, rate) is available for grass growth and the relevant intercepted radiation is calculated as:

$$Int.Rad_{GR} = 1 - \exp(-k \cdot LAI) \cdot (1 - Int.Rad_{OT}) \quad [11]$$

Where k is the extinction coefficient and LAI is grass cover leaf area index.

LAI growth for grass was modelled according to the approach proposed by Celette et al. (2010) [HC1]for simulating water balance of an intercropped vineyard (WaLIS model. Accordingly, daily potential LAI increase of grass cover (LAIgr) is calculated as the difference between the daily LAI increase (GLAId) and daily LAI senescence (SLAId):

$$LAI_{gr} = GLAI_d - SLAI_d \quad [12]$$

In not stressed conditions, GLAId is dependent on LAI growth rate of grass cover (LAI-rate, $m^2\ m^{-2}\ day^{-1}$) and Ft (unit less) that is calculated as a quadratic function of temperature, ranging between 0 (at 0 ºC) and 1 (at 18 ºC)

$$GLAI_d = LAI_{rate} \cdot Ft \quad [13]$$

The fraction of LAI produced each day ($GLAI_d$) is initialized with zero degree-days, and the thermal time during the life of this fraction is calculated daily as DDA included between 0 and 18°C. When the cumulated thermal time of any given fraction of LAI reaches the thermal time threshold set by the leaf duration crop input parameter (700°C DDA), this fraction is assumed to be senescent and it is subtracted from the total LAI.

2.1.3. Water balance and impact of water stress on potential growth

The soil was considered as a single finite reservoir consisting of two layers, where each layer is defined by its water content availability (WCA, i.e., the water included between field capacity and wilting point, $m^3\ m^{-3}$) and total transpirable soil water (TTSW) (i.e., WCA * rooting depth, mm). In order to consider the specific characteristics of a typical olive grove, which includes olive trees and grass cover, we defined a simplified soil system with two different overlaid soil layers as delimited by root system depth of these plants. The first is between soil surface and root depth of grasses, the second between root depth of grasses and maximum depth of olive tree roots. Accordingly:

$$TTSW = TTSW_1 + TTSW_2 \quad [15]$$

Soil water balance is tracked for each layer of the soil profile. A cascade model interconnects the two layers so that, if the amount of water entering the first layer exceeds its field capacity, the remaining water enters the layer below. Assuming no irrigation and no surface runoff, available soil water for each layer (ATSW, mm) depends on its value from the previous day as refilled by precipitation (Rain, mm), and depleted by evaporation from soil surface (SEVP, mm) and olive tree and grass transpiration (Tr_{OT}, Tr_{GR}). Given that grasses and olive tree root systems explore different soil depths and compete for water only in layer 1, ATSW in this layer was calculated on a day *d* as:

$$ATSW_1 = ATSW_{1(d-1)} + Rain \quad [16]$$

If the ATSW1 exceeds TTSW1, then the excess water enters layer 2. Accordingly:

$$ATSW_2 = ATSW_{2(d-1)} + (ATSW_1 - TTSW_1) \quad [17]$$

On the evidence that a stable response function exists between plant gas exchanges, as affected by extractable soil water content (Sinclair et al., 1998), we used the ratio between the actual water content (ATSW) and TTSW (i.e., fraction of transpirable soil water, FTSW) as index to rescale potential growth and leaf area for olive trees and grass cover. Accordingly, FTSW for layer 1 is calculated as:

$$FTSW_1 = ATSW_1/TTSW_1 \quad [18]$$

While FTSW over the entire profile (layer 1+layer 2) is calculated as:

$$FTSW_{1\_2} = (ATSW_1 + ATSW_2)/(TTSW_1 + TTSW_2) \quad [19]$$

The relative effect of FTSW on RUE (Red_Photo, rate) is calculated according to the general equation as proposed in Sinclair (1986):

$$\mathrm{Re}d\_Photo = \frac{1}{\left[1 + a * EXP\left(-b * FTSW\right)\right]} \quad [20]$$

as dependent on $FTSW_{1\text{-}2}$ for olive tree and on $FTSW_1$ for grass cover and used to rescale the relevant DM to their respective actual values (ADM_{OT}, ADM_{GR}) according to the same scheme:

$$ADM_i = DM_i \cdot Red\_Photo_i \quad [21]$$

Where the sub-index *i* refer to either olive trees (ot) or grass (gr)

FTSW affects also potential leaf area growth of olive tree (LAI_{inc}) and grass cover (GLAId).

In the first case, actual LAI_inc ($ALAI_{inc}$) is rescaled using the relationship between FTSW and leaf area growth (Red_LAI, see SI.1 for details):

$$ALAI_{inc} = LAI_{inc} \cdot Red\_LAI \quad [22]$$

In the second, actual daily LAI increase ($AGLAI_d$) is rescaled according to:

$$AGLAI_d = GLAI_d \cdot WIC \quad [23]$$

Where WIC is calculated as:

$$WIC = \max(0, \min(1, \frac{FTSW_1}{FTSW_{reg\_LAI}})) \quad [24]$$

Where $FTSW_{reg\_LAI}$ is water stress threshold for reducing leaf area growth, which was assumed as 0.48 (i.e. the breakpoint at which FTSW starts impacting RUE of wheat).

ADM calculated for both olive tree and grass cover is converted into transpired water (Tr_{OT}, Tr_{GR}, mm day^{-1}), according to the conservative relationship between crop transpiration and biomass production (Tanner and Sinclair, 1983; Sinclair et al., 1984): Accordingly:

$$Tr_i = ADM_i \cdot VPD/Kd_i \quad [25]$$

Where the sub-index *i* refer to either olive trees (ot) or grass (gr),

Where Tr (kg m-^{2} d^{-1}) is daily crop transpiration, VPD is daily water pressure deficit (kPa) and Kd (Pa) is a species dependent coefficient (transpiration efficiency coefficient, TEC).

Finally, at the end of day *n*, $ATSW_1$ and $ATSW_2$ are updated considering olive tree and grass cover transpiration and soil evaporation SEVP.

$$ATSW_1 = ATSW_1 - [Tr_{GR} + (Tr_{OT} \cdot sf1) + SVEP] \quad [26]$$

$$ATSW_2 = ATSW_2 - (Tr_{OT} \cdot sf2) \quad [27]$$

Where *sf1* and *sf2* are scalar factors to account for olive tree transpiration over the entire soil profile that is proportionally partitioned between layer 1 (*sf1*= thickness of layer 1 /maximum rooting depth) and layer 2 (*sf2*= thickness of layer 2/ maximum rooting depth).

Potential SEVP is calculated as evaporation from a wet soil surface using a simplified Penman equation (Soltani and Sinclair, 2012), where driving variables are vapor pressure curve versus mean temperature (DELT), incident daily solar radiation (SRAD), and soil albedo (SALB). SRAD is discounted to account for the interception of radiation by the plants canopy (olive tree + grass). This potential value is calculated for a rainfall event greater than 10 mm. If the number of consecutive days after this event is greater than 5, potential SEVP is rescaled as a function of the square root of time since the start of the dry spell (DYSE, number of days).

$$DELT = EXP(21.255 - 5304 / (273 + TMP)) \times (5304 / ((273 + TMP)2)))$$

$$SEVPpot = SRAD \times (1 - SALB) \times (1 - INT.tot) \times DELT/(DELT + 0.68)$$

$$SEVP = SEVP \times [(DYSE + 1)^{1/2} - DYSE^{1/2})] \quad [28]$$

2.1.4. Simulation of environmental stresses on final yield and alternate bearing

The model considers both water and heat stresses as reducing factors of HI.pot using a linear function that describes the progressive effect of these stresses on final yield. The results of Moriana et al. (2003) and Rapoport et al. (2012) were used to identify the cardinal values of this function for water stress, corresponding to FTSW below which water stress starts to affect final yield (*FTSWo*), and FTSW corresponding to yield=0 ($FTSWm$) (Fig. 14 in SI_2).

According to the results, the average FTSW calculated around anthesis ($FTSW_{ant}$) was used to linearly rescale HI.pot from its unstressed value (0.35) to its actual value ($HIws$) when $FTSW_{ant}$<0.4:

$$HIws = HI.pot * (1 - (FTSWo - FTSWant)/(FTSWo - FTSWm))$$

Where $FTSWo\ is\ 0.4\ and\ FTSWm = 0.05\ corresponding\ to\ HIws = 0$ (Fig. 14 in SI_2)

A similar approach was used to account for the impact of maximum temperatures at anthesis that were reported to affect pollination and fruit set for values higher than 30°C (*TMAXo*) (Ropoport, 2012). Accordingly, in the model, average Tmax around anthesis ($TMAX_{ant}$) was used to decrease linearly HI from its potential value to its actual value for $TMAX_{ant}$>30°C. Since not an extreme value corresponding to HI=0 ($TMax_m$) was retrieved in literature, it was assumed for $TMax_m$=35°C. Accordingly, when $TMax_{ant}>TMax_o$

$$HIhs = HI.pot * (1 - ((TMAXant - \mathrm{TMAXo})/(\mathrm{TMAXm} - \mathrm{TMAXo})))$$

Finally, the actual HI (*HIa*) is calculated as the minimum between *HIws* and *HIhs*

These meteorological events, when extreme, trigger the beginning of alternate bearing, i.e. an imbalance between vegetative growth and fruit production (Lavee, 2007), where a poor fruiting occurring on a year results into over-cropping and reduced vegetative growth during the following year. To account for this biannual trend, in the model we introduced a function simulating alternate bearing in response to stress events. Accordingly, to account for increased production in the year *n+1* following a stress on HI (*HIa*<0.35) in year *n*, the new *HI.pot* is increased by:

$$HI.pot = 0.35 + (0.35 - HIa)$$

While to account for reduced vegetative growth, partition coefficient to leaves (PC_{lf}) is decreased by:

$$\mathrm{PClf} = \mathrm{PClf.pot} \times [1 - (0.35 - HIa)]$$

The new $HI.pot$ may be subjected the same to stress on anthesis in the following year.
To account for the continuation of biannual trend on olive yield and vegetative biomass over a period, when $HIa > 0.35$:

$$HI.pot = 0.35 - (HIa - 0.35)$$

$$\mathrm{PClf} = \mathrm{PClf.pot} \times [1 + (HIa - 0.35)]$$

As an example, the implementation of this model on final yield is shown for a case study in Figure 12 in SI_2.

2.2. Model calibration and validation strategy

2.2.1. Phenology model

GDH requirement for bud break and the relevant *tb* were calibrated using the average bud break dates recorded in two contrasting climates, Follonica (warm, 2007-2010, site C in tab. 1 in SI_2) and Montepaldi (cold, 1996-1999, site B in tab. 1 in SI_2) that exhibit a relative advance (DOY 80) and delay (DOY 103) in the occurrence of the stage. For each site, the relevant meteorological data were previously averaged over the period of observation and *tb* for GDH accumulation was calculated as the threshold providing the lowest difference in GDH amount calculated form 1st of January to observed dates of the stage in the sites.

The UniChill model calibration for flowering phase was performed considering a range of ±30% around the default values of *a, b, d, e, Ccrit* and *FcritFlo* obtained by Chuine (2000) for olive trees, while *c* was explored in a range from 1 to 8 °C (Orlandi et al., 2004). The calibration and optimization of all parameters (*a, b, c, Ccrit, d, e, FcritFlo*) was reached considering the minimum value for RMSE using the Self-Organising Migrating Algorithm of the soma package (Clayden, 2014) in R software environment.

The model was calibrated on three different sites Florence (1993-2008), Lido di Camaiore (2001-2017) and Grosseto (2013-2017) (sites A, F, E in Tab. 1 of SI_2). The model calibrated for Florence was validated in a nearby site (Prato) in the period 1992-1998 (site D in Tab. 1 of SI_2). Given the absence of a validation site, the model for Lido di Camaiore was calibrated in 2001-2010 and validated in 2011-2017. The model for Grosseto was only calibrated given the short series of observations.

2.2.2. Growth model and sensitivity analysis

The literature was surveyed and used to parametrize the model. RUE for olive trees was obtained by averaging the results obtained over three consecutive years in Villalobos et al. (2006) (0.97 g dry matter MJ^{-1}). The relationships between FTSW and relative change in photosynthetic efficiency and

355 leaf area for olive trees were obtained from a specific experiment conducted on pot-grown olive trees
356 (see SI_1).
357 RUE of grass cover, which is represented by a typical forage mixture of species including grasses and
358 legumes as usually performed for grassland renovation (Argenti et al., 2012), was set to 2.2 g MJ
359 (Belanger et al., 1992; Duru et al., 1995; Soltani and Sinclair, 2012). The relationships between FTSW
360 and relative change in RUE and LAI growth were obtained from Schoppach and Sadok (2012) by
361 assuming grass cover behaving like wheat crop to water stress. Owing to the fact that natural grass
362 vegetation is highly adapted to the Mediterranean environment, we selected the FTSW threshold at
363 which transpiration started to decrease and the slope for this decrease relevant to the most tolerant
364 variety as representative of the drought-adapted natural grasses in the grove.
365 Dry matter partitioning coefficients to leaves (PClf.pot) in olive trees before anthesis was set to 25%
366 of daily assimilation (Mariscal et al., 2000), while after anthesis it was reduced to 9% to account for
367 the lowest priority in carbon allocation (Morales et al., 2016). The potential proportion of final yield
368 to total dry matter (potential harvest index, HI.pot) was obtained by Villalobos et al. (2006) for not-
369 limiting water conditions (0.35).
370 These coefficients were rescaled from the reported values in consideration that partitioning to roots,
371 which was not included in the original measurements, accounted for an additional 30% of total
372 produced biomass (Nardino et al., 2013).
373 Specific leaf area was set at 0.0042 m^2 g^{-1} (Villalobos et al., 2006).
374 Three parameters were calibrated, namely Kd for olive trees and grass and LAI-rate for grass using
375 NPP obtained in site 1 (Fig. 2, Tab. 1), where in a olive grove fluxes of carbon dioxide (CO_2), water
376 vapor (H_2O), sensible heat (H) and latent heat (LE) between the biosphere and the atmosphere where
377 monitored from 2010 to 2012. Specifically, the calibration was performed in 2010 by minimizing the
378 root mean square error (RMSE) between NPP observed and simulated in 2010. Kd for olive trees and
379 grass were iteratively tested in a range from 3 to 9 KPa (step 0.25) and LAI-rate for grass in a range

from 0.01 to 0.1 (step 0.01). For each iteration, the results for the entire orchard were compared to observed data cumulated per ten days and the coefficients minimizing the RMSE were selected. The calibrated model was then applied to simulated NPP of the entire olive grove in 2011 and 2012 in the same site (see SI_MAT_MET for details).

The calibrated model was further tested to assess its reliability in simulating specific processes of olive tree, grass cover growth and final yield. In site 2 and site 3 (Fig. 2, Tab. 1) the model was tested in simulating soil water dynamics (2013 and 2016) and transpiration (2012-2013). In site 4 (Fig. 2, Tab. 1), the model was tested in simulating LAI increase and final yield of olive trees under different treatments (rain fed, full irrigation and 50% deficit irrigation) from 2008 to 2010. In site 5 (Fig. 2, Tab. 1) the grass cover model was tested against daily growth rate of a typical Mediterranean mixed grass in 1994. In sites 7-13 the model was applied to simulate final yield on a farm level, in areas showing different elevations, climate, soils and planting density (Fig. 2, Tab. 1). Additional description of the sites and further details of the experiments may be found SI_MAT_MET.

Root mean square error (RMSE, equation 1 in SI_MAT_MET), correlation coefficient *R*, mean bias and absolute errors (MBE, MAE equation 2 and 3 in in SI_MAT_MET) were used as goodness[MM2] of fit indicators.

Latin hypercube sample (LHS) method was applied to explore the behavior of the calibrated model in response to a specific variation of its parameters or input values, using 1999 at site 1 as test case, considered as an average year of the area. Specifically, LHS is a regression approach that measures how strong the linear association is between the model output and each input parameter, while controlling the effect of the other factors (partial rank correlation coefficient, PRCC), (Confalonieri et al., 2010).

We tested the model sensitivity in terms of total yearly cumulated biomass of grass and olive trees to changes in physiological parameters (RUE, TE, LAI rate), grove architecture (inter-row and intra-row distances and crown dimensions), and soil parameters (root depth and AWC), by sampling in a range from -20% to +20% of their default values assuming a normal distribution.

406 The results are shown in terms of *PRCC* between a parameter or variable and the total biomass
407 accumulation of olive tree and grass cover.
408
409 Table 1. Sites description biblio fin qui
410
411 **3. Results**
412 *3.1. Phenology model*
413 The phenology model evidenced different calibration for olive tree cultivars adapted to cooler (inner
414 areas) and warmer (coastal areas) climate in Tuscany region (Table 1 in SI_2). For bud break, the
415 phenology simulation at Follonica (warmer site) was found 20 days-early compared to Montepaldi
416 (cooler site) with an average 3400 GDH accumulated using a base temperature (*tb*) of 8.5°C from 1st
417 of January.
418 For flowering phase, the results of model calibration and validation for flowering (Tab. 2 in SI_2)
419 evidenced high performances for all sites (Table 3 in SI_2). The end of endo-dormancy period in
420 coastal areas was reached around the end of December with 73 (Grosseto) and 77 (Lido di Camaiore)
421 CU accumulated. On the other hand, the inner areas reach the end of endo-dormancy period around
422 the first days of February with 80 CU accumulated in Florence (Table 2 in SI_2). The optimal
423 temperatures such as the development rates for chilling units accumulation were found higher for
424 experimental sites characterized by warmer winter temperature (i.e. 6.7°C at Lido di Camaiore and
425 5.5°C at Grosseto) compared to cooler winter temperature sites (Table 2 in SI_2). Finally, the eco-
426 dormancy period did not show significant differences between areas with 42, 44 and 45 FU
427 accumulated at optimal forcing temperature of 16, 15.6 and 15.5°C for Grosseto, Florence and Lido
428 di Camaiore, respectively (Table 2 in SI_2).
429
430
431

3.2. Growth model

The result of the optimization process indicated that the model performances, evaluated in terms of RMSE calculated with respect to NPP observed in 2010 cumulated over ten days, were mainly driven by change in growth rate of grass cover (LAI-rate) while the model was less sensitive to change in Kd of both olive tree and grass cover (Fig. 4 SI_2). According to the optimization procedure, LAI-rate, Kd for olive trees and grass were set to the values minimizing the respective RMSE, which corresponded to 0.024 d-1, 7.1 Pa and 3.9 Pa, respectively. Under this configuration, the relationship between observed and simulated data in 2010, cumulated per ten-days, yielded a RMSE of 9.9 g m^{-2} with an r = 0.75 (***) (Tab. 3). On a yearly basis, the model underestimated cumulated olive grove biomass (730 g m^{-2}) with respect to what was observed (827 g m^{-2}). Overall, ground cover represented 24% of total grove cumulated dry matter.

Interestingly, when looking at the daily course of observed NPP in 2010, the model was able to reproduce the drop of agroecosystem dry matter production as a consequence of soil tillage on DOY 135 that entirely removed the grass layer and was simulated by setting LAI of grass to 0. The following grass recovery, joint to assimilation rate of olive tree likely leaded to an assimilation peak on DOY 180 (Fig. 5 in SI_2).

The calibrated version of the model faithfully reproduced the seasonal trend of NPP when applied in the same grove in 2011 and 2012 (Fig. 3bc; Fig. 6bc in SI_2). In particular, the model satisfactorily simulated NPP in the validation datasets by detecting the effect of prolonged drought periods that occurred in both years, which reduced the observed assimilation rate of the grove with respect to 2010. Cumulated rainfall in 2011 and 2012, in fact, was 54% and 71% with respect to 2010 (697 mm), in the period included between January 1st and the harvest date (DOY 330). The lower rainfall, especially during the soil water recharge period (winter), resulted in a reduced biomass accumulation observed in both years with respect to 2010 with a total cumulated NPP of 642 in 2011 and 583 g m^{-2} in 2012. The model correctly simulated this trend, with a very good performance, especially in 2011. On a ten-days basis, the correlation between simulated and observed data yielded

458 an R=0.85 with an RMSE=5.2 g m^{-2}. On a yearly basis, the simulated olive grove cumulated NPP
459 (617 g m^{-2}) was close to the observed one (Tab. 3). Overall, ground cover represented 17% of total
460 grove cumulated dry matter.

461 In 2012, whereas the daily trend of NPP was well captured by the model (Fig. 3c), with two
462 main peaks detected in early and late spring, the model simulation resulted as overestimated with
463 respect to observed data, especially during the recovery in the early autumn. Consequently, on a ten-
464 day basis the performances were reduced with respect to 2011 with an R=0.76 and RMSE=6.8 g m^{-2}
465 (Tab. 3). Over the season, the model overestimated the cumulated NPP (639 g m^{-2}) with respect to
466 observed data (583 g m^{-2}) and this was especially due to an overestimation of autumn recovery.
467 Overall, ground cover represented 24% of total grove cumulated dry matter.

468 The calibrated model, was further tested to evaluate its performances in simulating daily
469 transpiration rate and daily soil water content for high-density groves in sites 2 and 4 (Figs. 4, 5, 6)
470 (Figs 7, 8, 9 in SI_2). The results for site 2 indicated that the model correctly simulated the daily
471 course of FTSW in the layer explored by both grasses and olive tree root systems (0-25 cm, r=0.94,
472 RMSE=7.5%) and the entire soil layer (1 m, r=0.95, RMSE=11%) (Tab. 3) (Fig. 4ab) (Fig. 7 in SI_2).

473 Similar performances were observed in site 4 (Fig. 6ab), where FTSW in the soil profile was
474 satisfactory simulated with a slight overestimation for layer 1 (r=0.94, RMSE=6.5%) and
475 underestimation for layer 2 (r=0.91, RMSE=9.9%) (Tab. 3) (Fig. 9 in SI_2).

476 The good performances in simulating water balance at different depths and in different locations
477 were further corroborated by the good simulation of olive tree daily transpiration rate in site 2 in 2012
478 and 2013 (Fig. 5). The model correctly simulated the depressing effect of drought stress at the end of
479 the growing season in 2012, the increasing trend of transpiration observed in 2013 at the start of
480 growing season due to abundant rainfall (from DOY 100 to 122), and the progressive effect of drought
481 in summer. Nevertheless, the model slightly underestimated transpiration (Tab. 3) (Fig. 8 in SI_2).

482 In sites 2 and 4, cumulated ground cover dry matter represented 16% and 23% of total grove
483 dry matter accumulation.

The results obtained for site 1 and 3 indicated the overall good performances of the model in the simulation of total biomass accumulation (r=0.92, RMSE=1.83 Mg ha^{-1}) and final yield (r=0.94, RMSE=0.71 Mg ha^{-1}) (Tab. 3), considering 2011 and 2012 for site 1 and 2008, 2009 and 2010 for site 3 (Fig. 7). In site 3, cumulated ground cover dry matter represented on average 20%, 18% and 14% of total grove dry matter accumulation in fully irrigated, 50% deficit irrigation and rain fed treatments.

The yearly LAI increment recorded in site 3 pointed out that the model correctly detected the trend of LAI increase (i.e the difference between LAI at the end and the beginning of the season) over the studied period (Fig. 10 in SI_2) but it was slightly underestimated.

When applied over farm sites, the model satisfactorily simulated inter annual yield variability (Fig. 8), showing a RMSE=0.4 Mg DM ha^{-1} (Tab. 3).

In site 5, the grass cover model captured the observed trend of grass growth with a main peak in early spring, and a secondary one in autumn, even though in advance with respect to observed data (Fig. 9). Overall, the model provided good performances in terms of r (0.94) and RMSE (5.6 kg ha^{-1} day^{-1}) (Fig. 11 in SI_2).

Table 3. Goodness of fit indicators for simulations over sites 1-5. Legend: FTSW1 relates to data from the 0-20 cm layer; FTSW relates to the entire soil layer.

3.3.Sensitivity analysis

The LHS indicated that olive and grass biomass accumulation were highly sensitive to intercepted radiation parameters with a clear interaction between the agro-ecosystem elements. Increase in plant density of olive tree and crown dimensions, in fact, positively influenced olive tree biomass accumulation while it reduced the accumulation of grass cover as the effect of increasing

shading by trees. In particular, the crown diameter was the most influencing factor for biomass accumulation while the grass LAI rate was the parameter most influencing its biomass accumulation with a low negative interaction with olive biomass accumulation (Fig. 10).

Both RUE and Kd of olive trees and grass cover were the positively related to biomass accumulation of relevant components, where in general the model was more sensitive to RUE than to Kd. Both grass and olive biomass are positively related to AWC and the relevant soil depth.

The analysis emphasizes the completion between the grass cover and olive tree for radiation and water as outlined by the positive effect of increased plant density on grass growth and the negative impact of increasing grass root depth and LAI rate on olive growth.

4. Discussion

A new olive grove model, based on process-based algorithms, was designed to simulate phenology, biomass accumulation and yield, and competition with ground cover. The model was developed bearing in mind that process-based models usually require the calibration of multiple parameters and need many input variables to provide reliable results. These major requirements for input data and parameters makes the approach not readily applicable on a local scale either for operational purpose or on a regional scale for planning strategies (Challinor, 2004; Soltani and Sinclair, 2011). Instead, simple process models that require fewer input variables may find a wide application, especially for operational purposes, if they are based on a robust approach but are usually limited to the range of their calibration dataset (Montheith, 1996).

With these premises, we developed the model by limiting the required input data and parameters to set it up. In addition, to ensure its wide applicability, calibration and validation were performed on sites having contrasting weather and climate (within the Mediterranean area) as well as different soils, planting density and management practices.

The simulation approach originally developed in Sinclair (1986) and Amir and Sinclair (1991) for crops and modified by Bindi et al. (1997) and Bindi et al. (2005) for grapevine, uses RUE and

536 transpiration efficiency coefficient Kd as the main parameters driving the simulation of daily dry
537 matter assimilation. A simple but straightforward empirical approach was used to describe the
538 relationships between the fraction of transpirable soil water (FTSW) and both leaf area growth (LA)
539 and transpiration (TR) in olive trees for a widely cultivated Tuscan variety (cv Leccino). Interestingly,
540 the results in SI_1, indicated that the FTSW thresholds limiting leaf area growth and transpiration
541 were approximately the same (0.31) but after this threshold, leaf area growth was more sensitive to
542 FTSW decrease than transpiration rate. This may further emphasize the productive strategy that olive
543 tree implements under a water stress regime, where leaf expansion is reduced to avoid water loss and
544 preserve photosynthesis (Casadebaig et al., 2008). This in contrast to the "conservative strategy",
545 which aims at reducing leaf expansion when FTSW is still relatively high (Sinclair and Muchow,
546 2001).

547 The few parameters required for the model (Tab. 3), many of which were found in the literature,
548 further simplified the calibration that was limited to three parameters, (Kd for olive tree and grass
549 cover, and LAI growth-rate of grass). This is highly desirable to avoid a model with too large a set of
550 crop-specific parameters to be calibrated that would result in a likely best fit for a particular site but
551 with results that could hardly be extrapolated to another site without readjustment of the model
552 coefficients (Sinclair and Seligman, 2000).

553 Tuscany region was selected as testing area for the model. This region, which coincides with
554 the northern limit of olive tree cultivation in Italy (Moriondo et al., 2008, 2013), shows very
555 heterogeneous climatic features (Rapetti and Vittorini, 1995) as well as soil types and management
556 practices, so it is suitable for testing the applicability of the proposed model. Its climate ranges from
557 Mediterranean to temperate warm or cool following altitudinal and latitudinal gradients and distance
558 from the sea (Rapetti and Vittorini, 1995). In particular, the most southern, coastal provinces Grosseto
559 (sites 1, 2, 3, 6) and Livorno (site 8) are the warmest and driest, while the inner provinces Florence
560 (site 4, 10, 11), Siena (site 13) and Lucca (site 7) have a more continental climate. The sites used for
561 calibration and validation are characterized by different planting density (from 250 to 500 plants ha^{-}

562 [1]), soil conditions (from sandy to clay-loam) and management practices (rain fed, irrigation, deficit
563 irrigation), making the dataset a summary of climates and practices used for olive trees across the
564 Mediterranean basin.

565 The results obtained in the calibration/validation tests emphasized the robustness of the model
566 in simulating the assimilation performances of the entire ecosystem, as well as growth and
567 development of the single ecosystem components.

568 The phenology model results were obtained using bud-break and flowering dates that are not
569 related to specific varieties but rather they are representative of varieties pool adapted to different
570 climate conditions. The olive trees in the coastal area showed a shorter dormancy period that
571 culminated with an earlier bud-break and flowering compared to inner areas. Indeed, budbreak occurs
572 20 days-earlier for warmer site (Follonica, site C in in SI_2) compared to the cooler site (Montepaldi,
573 site B in SI_2). This phenomenon is driven by warmer temperatures that promotes an earlier opening
574 of vegetative buds in Follonica compared to the Montepaldi site.

575 The flowering stage was simulated accounting the dormancy period during which the
576 differentiation between vegetative and reproductive buds occurs (De Melo-Abreu et al., 2004; Orlandi
577 et al. 2004; Fabbri and Alerci, 1999). Our results evidenced three different phenology responses,
578 especially during the endo-dormancy period, for experimental sites characterized by different climate
579 conditions. In warmer areas, the temperature threshold for chilling accumulation were higher (6.7°C
580 and 5.5°C for Lido di Camaiore and Grosseto) with respect to inner colder areas (2.90°C for
581 Florence). These results are in accordance with Aguilera et al. (2014) that highlights significant
582 differences in the peak of chilling unit accumulation from northern and southern sites with a shorter
583 endo-dormancy period for locations situated at lower latitudes.

584 The overall growth model (i.e. ground cover + olive tree layer) was calibrated and validated
585 using carbon flux data from the EC technique. These data can be considered particularly suitable for
586 assessing process-based model performances since they take into account the effect of weather and
587 management practices on the ecosystems at the scale required to evaluate the performances of a

588 process-based model (i.e. from half-hour to daily). The three years used in the calibration/validation
589 process with EC data included 2012 that was observed to be close to the long-term average (i.e. 1981-
590 2012) yearly rainfall (626 mm y^{-1}; anomaly=-0.3%), while 2010 and 2011 represent positive
591 (anomaly=+27.4%) and negative extremes (anomaly=-41.3%) (Brilli et al., 2016). As such, these data
592 can be considered a reliable benchmark for testing the model performances.

593 The calibration process resulted in a Kd for olive tree (7.1 Pa) close to what was observed for
594 grapevine in a Mediterranean climate (6 Pa, Bindi et al., 1996), supporting olive tree efficiency in
595 water use (Xiloyannis et al., 1999) as an effect of physiological adjustments and morphological
596 adaptations (Moreno et al., 1996; Chartzoulakis et al., 1999; d'Andria et al., 2009; Tognetti et al.,
597 2009; Cocozza et al., 2015). Kd for grasses was lower than that observed for olive tree (4 Kpa) and
598 within the range for C3 species reported in Soltani and Sinclair (2011).

599 EC data have already been used extensively for model calibration and validation (Brilli et al.,
600 2017). They were widely used especially for assessing carbon and nitrogen dynamics between
601 ecosystems (i.e. arable, paddy soils, grasslands, forests, savanna, etc.) and the atmosphere (Congreves
602 et al., 2016; Noirot-Cosson et al., 2016; Giltrap et al., 2015; Brilli et al., 2014; Fitton et al., 2014ab;
603 Li et al., 2010). However, since from the EC data used in this paper it was not possible to disentangle
604 the dynamics of each single component, the performances of the calibrated model were evaluated in
605 simulating specific processes obtained separately for grass and tree cover (i.e. olive tree leaf area
606 growth and transpiration, evapotranspiration, total biomass accumulation of olive tree and grass and
607 final olive yield).

608 Unfortunately, reference ground biomass was not determined during experiments in sites 1, 2,
609 3, 4 and there is still not a consolidated literature on biomass partition between olive trees and grass
610 in groves. In any case, some comparisons may be attempted. Scandellari et al. (2016) reported that
611 ground cover represented 22% of total cumulated biomass for an intensive partially irrigated olive
612 grove (513 plants ha^{-1}, Gucci et al., 2012; Caruso et al., 2013), while Nardino et al. (2013) indicated
613 a higher ratio (35%) for a fully irrigated low-density grove (250 plants ha^{-1}). Our results, even though

614 they may not be fully comparable to these data because of different climate conditions, treatments
615 and planting density, are in line with this limited set of observations. In general, observed data
616 indicated that the contribution of ground cover to olive grove biomass tends to increase as planting
617 density decreases and this effect is fully simulated. Site 1, with a low planting density (250 plants ha^{-1})
618 (not irrigated), showed a range between 26% (2010, 2012) and 17% (2011), while in groves at
619 higher density (513 plants ha^{-1}, sites 2, 3, 4) as in Scandellari et al. (2016), the percentage ranged
620 from 13% in site 3 (rain fed treatment) to 22% in site 4 (rain fed). As an additional example, when
621 we decreased the plant density in site 3 from 513 to 256 plants ha^{-1} in a fully irrigated treatment to
622 reproduce the experiment in Nardino et al. (2013), the contribution of ground cover to olive grove
623 biomass increased from 20% to 37%, which is fully comparable to what was observed in that
624 experiment.

625 The simulation obtained in site 5 where, in the absence of tree cover, the model was able to
626 identify the timing and magnitude of maximum growth intensity and the following senescence period,
627 strengthens the previous results. The model simulated grass recovery in autumn, in advance with
628 respect to observed data, as the effect of prolonged rainy periods. These differences are likely related
629 to the presence in the plot of annual self-reseeding species, such as *Trifolium subterraneum* or *Lolium*
630 *rigidum*, typical of the Mediterranean area, which after senescence produce seeds that pass the
631 summer buried in the soil (Ghamkhar et al., 2015). This protection mechanism against drought
632 prevents a prompt response of the ground cover to sporadic rainfall events during summer ("false
633 breaks") when optimal conditions for seed growth are not yet reached (Koukoura, 2007). This
634 behavior, as many others that are not properly addressed by many grass models (Calanca et al., 2016),
635 is important for understanding the different responses observed in the field and are of great
636 importance when the simulation should represent competition for water between trees and grasses in
637 dry areas (D'Onofrio et al., 2015).

638 Simulations in site 1 indicated that the overall biomass partitioned to leaves was 13% in 2010
639 and 2012 and 15% in 2011. This result was consistent with independent data (Villalobos et al., 2006;

640 Sofo et al., 2005), which showed that, in not limiting water conditions, 11% and 9% of total yearly
641 cumulated biomass is invested in leaves. Similar results were obtained in sites 2, 3 and 4 (data not
642 shown). In any case, Mariscal et al. (1998) evidenced that in olive tree, biomass partition coefficient
643 to leaves decreases as planting density increases, but the implementation of such an effect still
644 requires further analysis since available research does not allow an estimation of this effect in the
645 field.

646 The robustness of the model was further emphasized by its capacity to simulate specific
647 processes such as olive tree transpiration and water dynamics in different soil layers, biomass
648 accumulation and ground cover growth. In sites 2 and 3, the model faithfully simulated the olive tree
649 transpiration and FTSW at 10 and 30 cm, demonstrating the ability of the model to reproduce the
650 actual evapotranspiration for different plant density, climate and soil. It also well reproduced the
651 effect of grasses and olive trees competition for water in the upper layer and more in general through
652 the entire soil profile.

653 The model applied on site 3, reproduced well total biomass accumulation and yield of an
654 intensive grove with three irrigation treatments. These good performances on experimental plots were
655 corroborated when the model was applied for yield estimation on farm level on sites 6-13. In
656 particular, yield data for these sites exhibited a general trend to alternate bearing (SI) that was well
657 captured by the model, highlighting the good performances of the proposed sub model (Fig. 12 in
658 SI_2).

659

660 Despite the good performances of the model in different environmental conditions, some
661 drawbacks and warnings in the use of present model due to a specific parametrization must be
662 highlighted.

663 There is still a lack in the understanding of processes underlying the release of bud break
664 (López-Bernal et al., 2017) and this limits the application of the proposed model. More in general,
665 given the large influence of climatic conditions on the parametrization of the phenology model,

666 further calibrations for its application outside the range of conditions where it was developed are
667 required.

668 The use of empirical approach describing the effect of FTSW on olive transpiration requires, in
669 any case, a different parametrization depending on the varieties that may exhibit different tolerance
670 to water stress (Cola et al., 2015). As an example, transpiration of cv "Coratina" grown in pots (Sofo
671 et al., 2008) showed a higher susceptibility to water stress than cv Leccino (this study), while cv
672 "Nocellara del Belice (Rallo and Provenzano, 2013) showed an intermediate response (Fig. 13 in
673 SI_2).

674 The sub-model describing the effect of heat and water stress at anthesis of final yield must be
675 refined as based on a limited number of observation to date present in literature.

676 The sensitivity analysis highlighted that olive tree growth is highly responsive to light
677 interception parameters (planting density, crown radius) and actually the model provided the highest
678 simulation performances when this information was available at a high spatial and temporal resolution
679 (site 3). When the model was feed with a lower quality data of ground cover as obtained from not
680 updated low-resolution imageries, the performances were significantly reduced (sites 6-13 Fig. 8,
681 Tab. 3). This implies that these parameters cannot be easily assumed but should actually reflect the
682 current situation in the olive grove. Proximal sensing data from an unmanned aerial vehicle (UAV)
683 could be exploited for such a purpose to derive the geometrical parameters of the canopy and LAI at
684 the highest spatial resolution (Caruso et al., 2017; Zarco-Teiada et al., 2014; Matese et al., 2017).

685 **5. Conclusion**

686 The objective of this work was to develop and validate a simple growth model simulating
687 growth of olive trees and grass cover. The model was calibrated and validated in Tuscany region over
688 sites encompassing different types of Mediterranean climate, soil and management practices. Overall,
689 despite having a simple architecture, it faithfully simulated different processes, including olive tree
690 phenology, plant transpiration and total biomass accumulation and partitioning at both tree and grass
691 level. This model can be therefore considered for monitoring of the current season trend over different

areas of the Mediterranean basin, especially for those areas where many input parameters are not readily available.

6. Acknowledgments

This research was supported by the LIFE project ADAPT2CLIMA ref: LIFE14 CCA/GR/000928

Tables

Table 1. Sites description. Legend: L=var. Leccino, F=var. Frantoio, M=var. Moraiolo; Tr=subclover, Fe=tall fescue, Lo=ryegrass; * not applicable; Tavg=average yearly temperature, TxHM= average maximum temperature of warmest month; TnCM=average minimum temperature of the coldest month; PP= average yearly cumulated rainfall; 1=soil data were extracted from the regional database described in Gardin and Vinci, (2016) reporting soil texture and depth. Soil texture was converted into soil AWC using pedo-transfer function (Saxton et al., 1986)

id	name	Experimental period	Lat N Lon E	elevation	varieties	Area	Plant spacing	Ground cover	soil AWC[1]	Soil depth[1]	T_{avg}	T_{xHM}	T_{nCM}	PP
			(°)	(m asl).		(ha)	(m)	(%)	(%)	(m)	°C	°C	°C	mm
1	S. Paolina (CNR)	2010-2012	42.93-10.77	10	L, F, M	6	7×5	25	17	1.1	15.45	29.54	4.18	614
2	S. Paolina (CNR)	2012-2013	42.93-10.77	10	L	0.1	4×4	33	17	1.1	15.46	30.40	4.61	695
3	Venturina (UNIPI)	2008-2010	43.02-10.61	10	F	0.5	4.3×4.3	37	11	1.5	15.08	29.25	3.65	1016
4	Florence (ITAS)	2016	43.78-11.22	80	F	0.5	7×5	38	16	1	15.94	34.14	2.8	964
5	Paganico	1993	42.93-11.27	340	Tr,Fe,Lo	*	*	*	11	1	14.67	28.67	2.72	846
6	Follonica	1970-1986	42.93-10.77	10	L, F, M	1.5	7×5	20	16	1.1	15.35	29.07	3.80	631
7	Capannori	2002-2006	43.89-10.61	75	L, F, M	1.2	7×5	24	17	1.4	14.46	30.47	0.77	1067
8	Bibbona	1998-2006	43.27-10.60	25	L, F, M	2.3	7×5	23	12	1.4	15.43	29.88	3.51	530
9	Roccastrada	1998-2006	42.97-11.14	23	L, F, M	2.2	5×5	28	16	1.1	15.51	33.68	2.38	745
10	Londa	2001-2006	43.84-11.51	250	L, F, M	1.6	7×5	22	15	0.79	14.17	31.31	0.76	948
11	Vinci	1998-2006	43.79-10.94	260	L, F, M	1.5	7×7	24	11	0.76	14.18	29.71	1.92	832
12	Castiglione D'Orcia	1999-2006	42.99-11.62	350	L, F, M	1.2	7×5	19	15	0.73	13.67	28.89	1.4	662
13	Loro Ciuffenna	1999-2006	43.59-11.61	600	L, F, M	0.8	7×7	20	11	0.76	13.39	30.41	0.16	835

705 Table 2. List of model variables

Variable	Description	Layer	Units/Value	Reference
State				
DM	Potential cumulated dry matter	OT/GR	g m^{-2}	
ADM	Actual cumulated dry matter	OT/GR	g m^{-2}	
LAI	Leaf Area Index	OT/GR	m^2 m^{-2}	
Yield	Yield per hectare	OT/GR	g m^{-2}	
Rates				
Int.Rad	Intercepted radiation	OT/GR	Rate (0-1)	Testi et al. (2005):
LAI_{inc}	Potential LAI growth	OT	m^2 m^{-2}	
$GLAI_d$	Potential LAI growth	GR	m^2 m^{-2}	Celette et al. (2007)
$ALAI_{inc}$	Actual LAI growth	OT	m^2 m^{-2}	
$AGLAI_d$	Actual LAI growth	GR	m^2 m^{-2}	
SLAId	LAI senescence rate	GR	m^2 m^{-2}	
LAI_rate	daily growth rate	GR	Rate (0-1) [0.023)]	*calibrated*
Red_photo	Effect of FTSW on RUE	OT	Rate (0-1)	*calibrated*
Red_photo	Effect of FTSW on RUE	GR	Rate (0-1)	Schoppach and Sadok (2012)
Red_LAI	Effect of FTSW on LAI growth	OT	Rate (0-1)	*calibrated*
FTSW	Fraction Transpirable Soil Water	OT/GR	Rate (0-1)	
$FTSW_{reg\_LAI}$	Fraction Transpirable Soil Water (break point)	GR	0.48	Schoppach and Sadok (2012)
ATSW1-2	Actual total soil water	OT/GR	mm	
Tr	Transpiration	OT/GR	mm d^{-1}	
HI.pot	Harvest index	OT	0.35	Villalobos et al. (2006)
SVEP	Soil evaporation	SO	mm d^{-1}	
PCf	Partition coefficient to leaves	OT	Rate (0-1) [0.27, 0.09]*	Marsiscal et al. (2000) Morales et al. (2016)
Plant parameters				
vol	crown volume	OT	m^3	
PlantA	m^2 per plant	OT	m^2	
Root depth	Max explored depth	OT	m	
Root depth	Max explored depth	GR	m	
k’	Olive tree extinction coefficient	OT	Rate (0-1)	Villalobos et al. (2006)
k	Grass cover extinction coefficient	OT	0.5	*assumed*
RUE	Radiation Use Efficiency	OT	0.97 g MJ^{-1} m^{-2}	Villalobos et al. (2006)
RUE	Radiation Use Efficiency	GR	2.2 g MJ^{-1} m^{-2}	Belanger et al., 1992 ; Duru et al., 1995
Kd	Coefficient	OT	7.1 Pa	*calibrated*
Kd	Coefficient	GR	3.9 Pa	*calibrated*
SLA	Specific leaf area	OT	0.0042 m2 g-1	Villalobos et al. (2006)
LAD	Leaf Area Density	OT	m^2 m^{-3}	
Soil parameters				
TTSW	Total Transpirable Soil Water	SO	mm	
AWC	Available Water Content	SO	mm	
Environmental parameters				
Tmin	Minimum daily temperature		°C	
Tmax	Maximum daily temperature		°C	
Rainfall	Daily cumulated rainfall		mm	
radiation	Daily global radiation		MJ	
VPD	Vapor Pressure Deficit		KPa	

Table 3 goodness of fit indicators for simulations over sites 1-13. Legend: FTSW1 relates to data from the 0-30 cm layer, FTSW relates to the entire soil layer. In the field *period*, the time spanning * indicates the first year and the last year considering all the sites. In the *aggregation* field, C=cumulated, A=averaged. The field *Fig* reports the number of figure in SI relevant to that variable and year showing the plot simulated versus observed data.

Site	**Variable**	**Period**	**Fig**	**Aggregation**	**R**	**RMSE**	**MBE**	**MAE**
1	NPP	2010		ten days (C)	0.75	9.9 g m^{-2}	-2.6 g m^{-2}	8.9 g m^{-2}
1	NPP	2011		ten days (C)	0.85	4.9 g m^{-2}	-0.58 g m^{-2}	4.14 g m^{-2}
1	NPP	2012		ten days (C)	0.76	6.3 g m^{-2}	--1.6 g m^{-2}	5.1 g m^{-2}
2	FTSW1	2013		ten days (A)	0.95	7.7%	3.6%	6.5%
2	FTSW2	2013		ten days (A)	0.96	11.0%	-4.7%	8.3%
2	Tr	2012-2013		ten days (C)	0.92	4.02 mm	-1.94 mm	3.16 mm
3	yield	2008-2010		year	0.94	0.53 Mg ha^{-1}	0.15 Mg ha^{-1}	0.44 Mg ha^{-1}
3	Total biomass	2008-2010		year	0.92	1.83 Mg ha^{-1}	-0.92 Mg ha^{-1}	1.60 Mg ha^{-1}
3	LAI	2008-2010		year	0.82	0.09	-0.08	0.08
4	FTSW1	2016		day	0.91	10%	-7.5%	7.3%
4	FTSW2	2016		day	0.94	6.5%	2.3%	5.1%
5	Grass biomass	1994		ten days (C)	0.96	5.6 Kg m^{-2}	2.7 Kg m^{-2}	4.45 Kg m^{-2}
6-13	yield	1970-2006*		year	0.77	0.41 Mg ha^{-1}	0.05 Mg ha^{-1}	0.3 Mg ha^{-1}

Figures

Figure 1. Flow diagram of the model including the simulation of olive tree and grass cover growth.

Figure 2. Experimental sites distribution in Tuscany region with relevant Thornwhite climate classification

Figure 3. Daily trend of observed and simulated NPP of S. Paolina olive grove in 2010 (a), 2011 (b) and 2012 (c), site 1 in table 1 and figure 1.

Figure 4. Daily course of observed and simulated FTSW in 2013 at site 2 at 30 cm and 10 cm.

Figure 5. Daily course of observed and simulated transpiration at site 2 in 2012 and 2013.

Figure 6. Daily course of observed and simulated FTSW in 2016 at site 4 at 30 cm and 10 cm

Figure 7. Correlation between observed and simulated total dry matter (a) and final yield (b) at sites 1 (2010-2012, closed circles) and 3 (2008-2010, open circles).

Figure 8. Yield simulation for sites 6 to 13 (fig. 2)

Figure 9. Daily course of observed and simulated grass productivity at site 5.

Figure 10. Model sensitivity analysis. Partial rank correlation coefficient for total cumulated olive tree (a) and grass (b) biomass. Standard error is indicated.

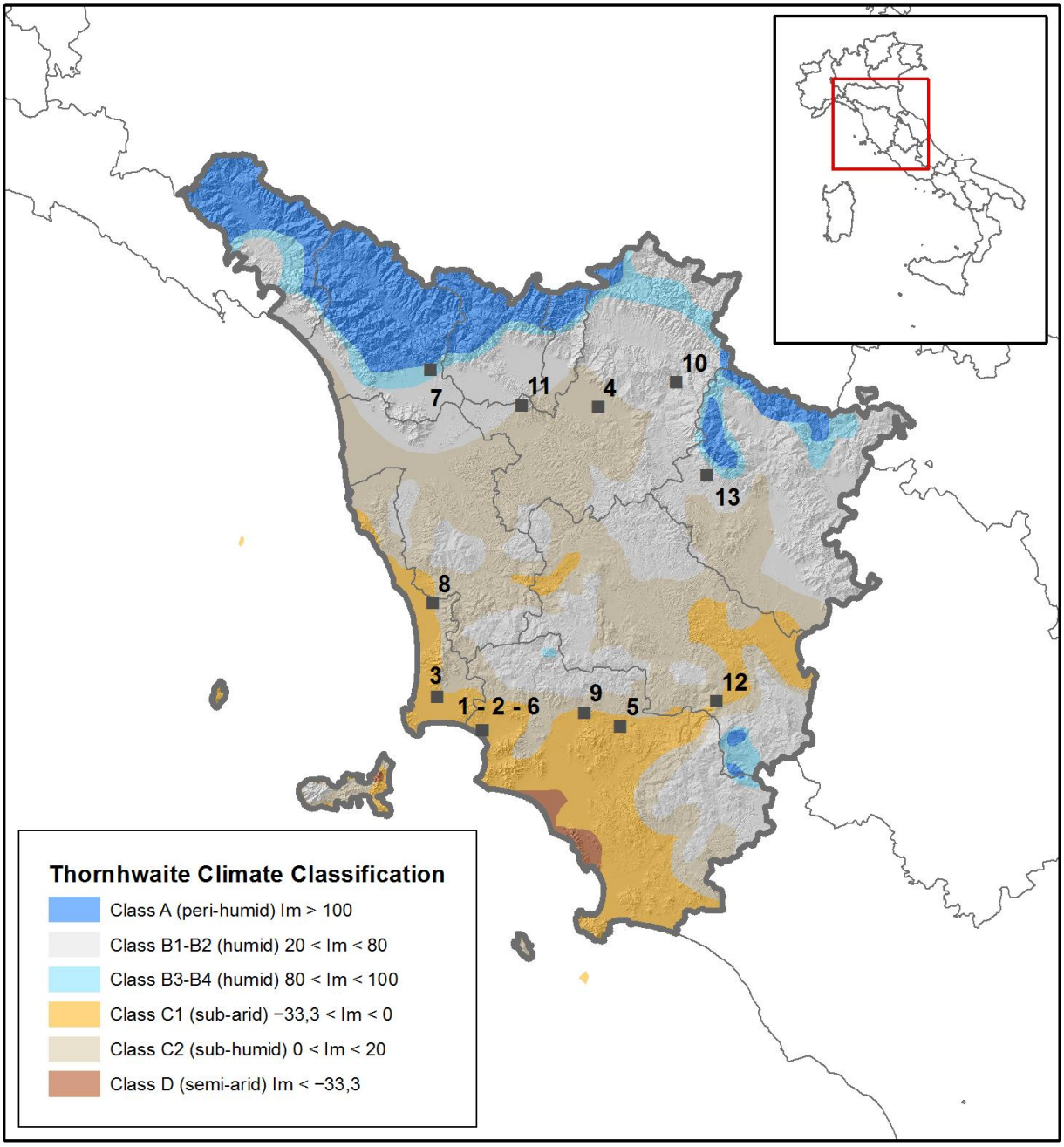

740
741 Figure 1

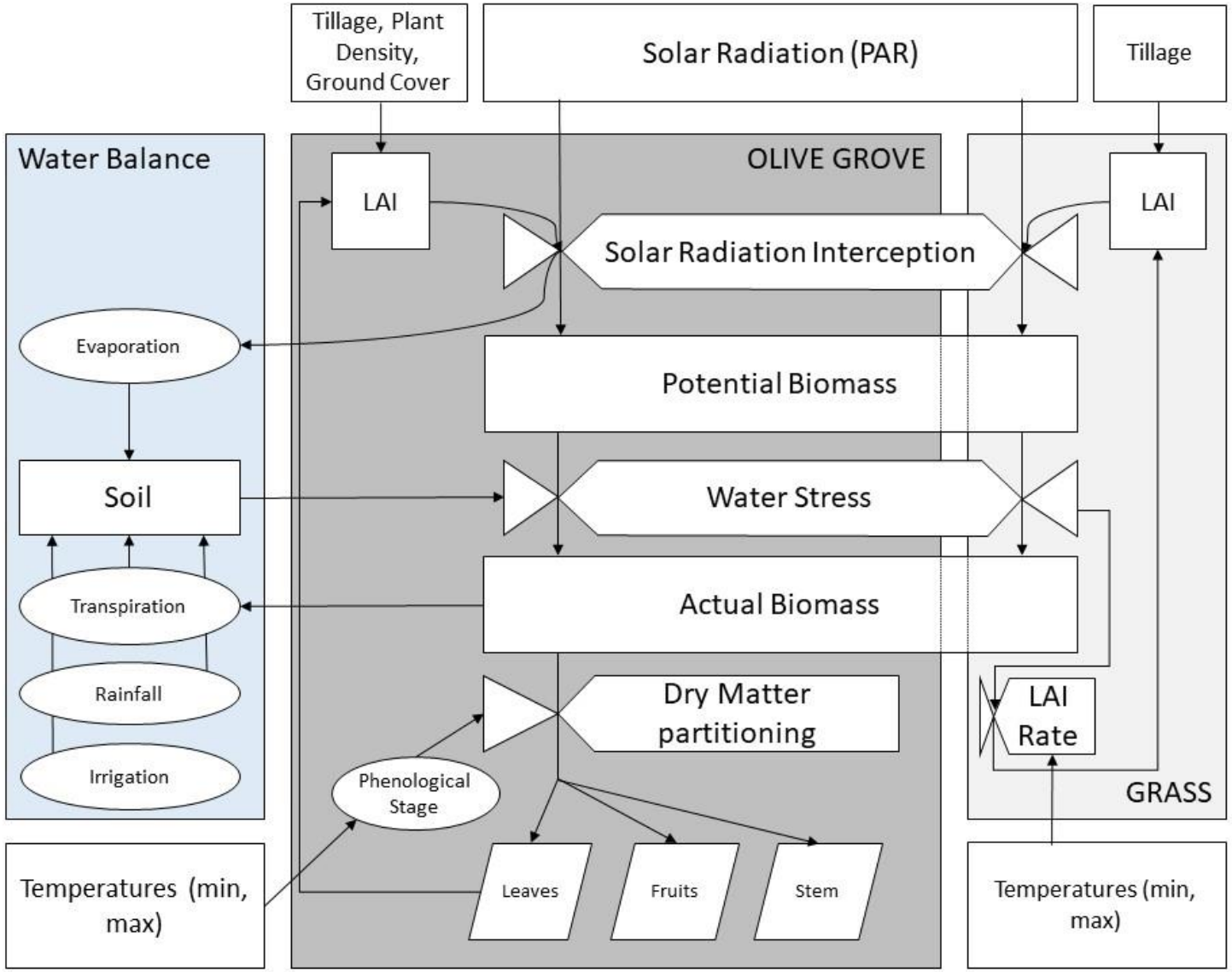

742
743
744 Figure 2

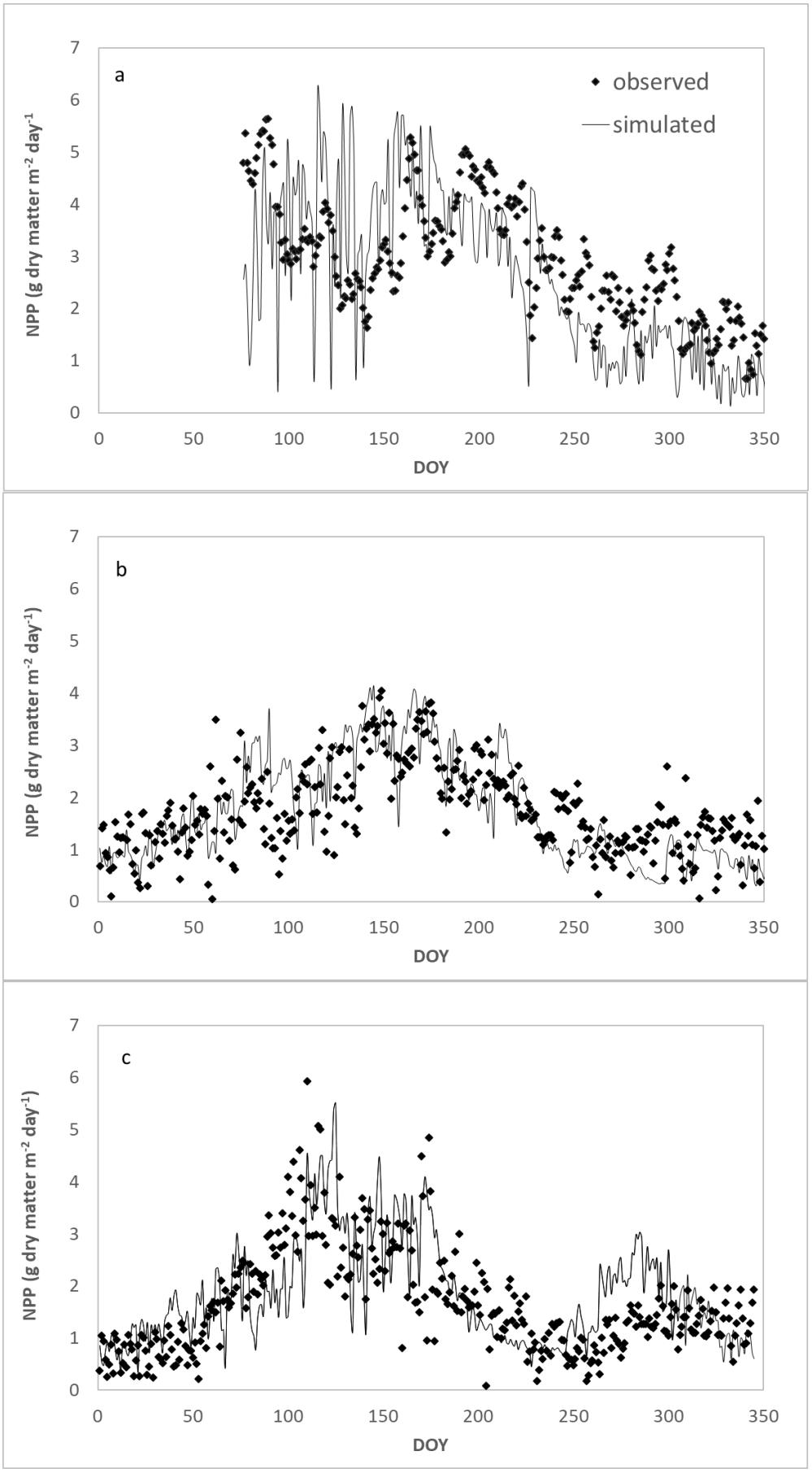

745

746 Figure 3

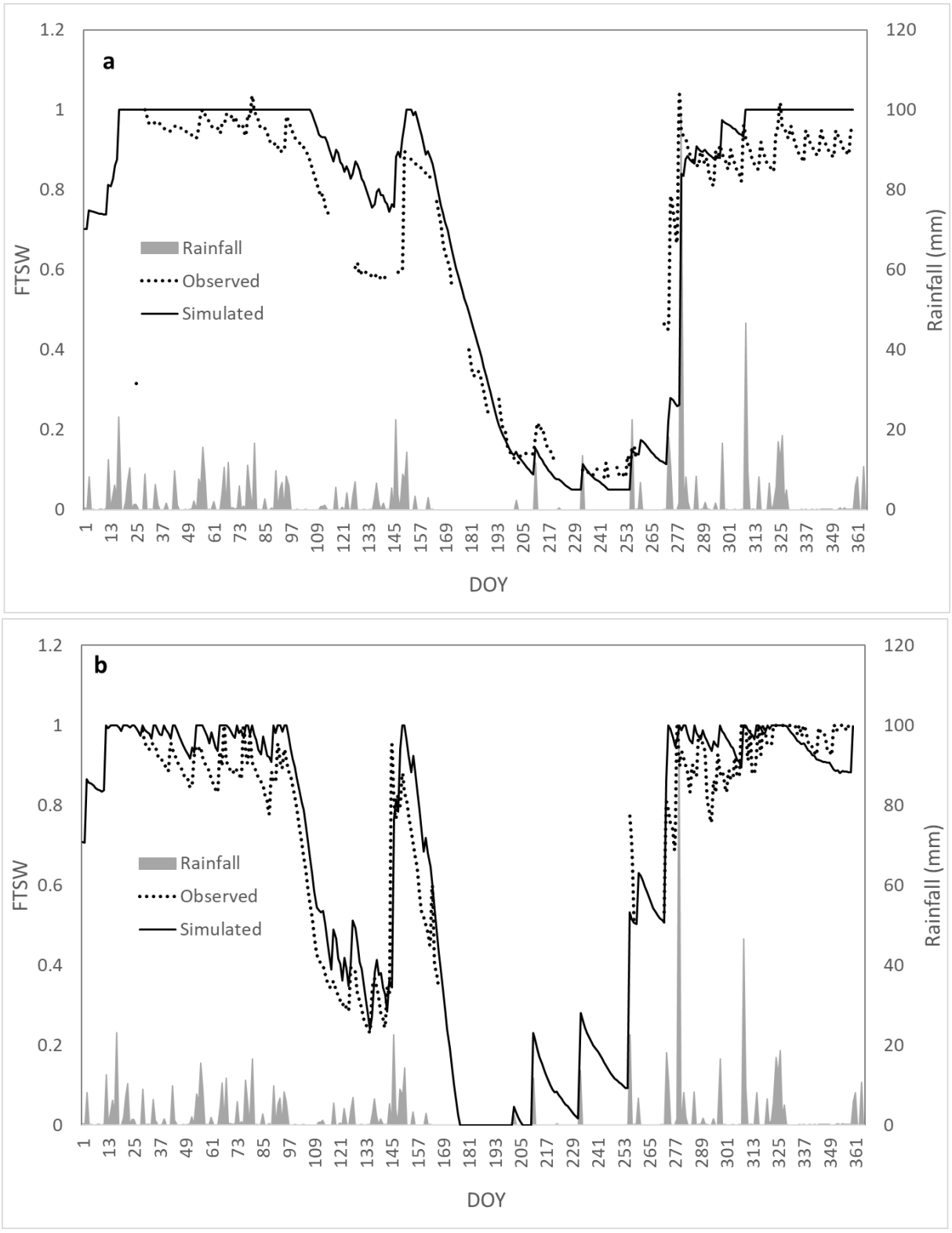
a
b
FTSW
Rainfall (mm)
DOY
Rainfall
Observed
Simulated
0
0.2
0.4
0.6
0.8
1
1.2
0
20
40
60
80
100
120
1
13
25
37
49
61
73
85
97
109
121
133
145
157
169
181
193
205
217
229
241
253
265
277
289
301
313
325
337
349
361

Figure 4

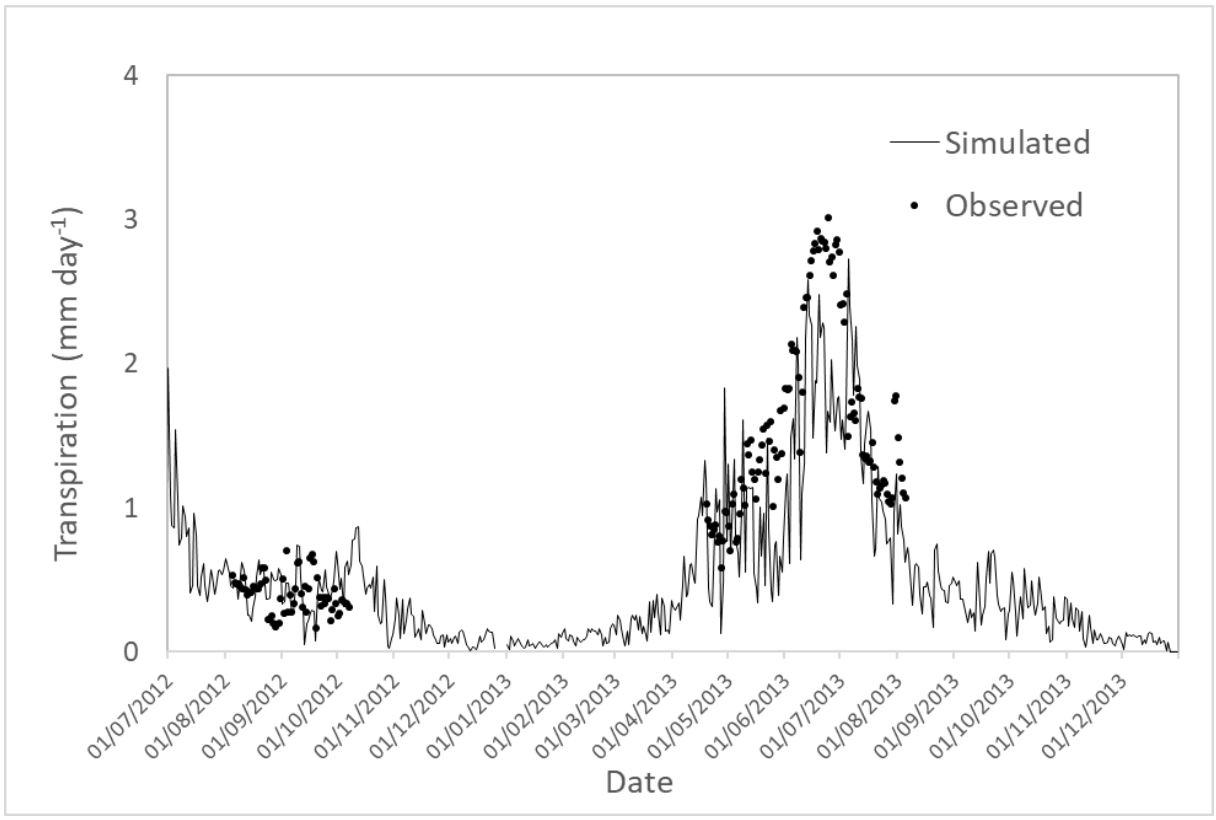
Transpiration (mm day-1)
4
3
2
1
0
Simulated
Observed
01/07/2012
01/08/2012
01/09/2012
01/10/2012
01/11/2012
01/12/2012
01/01/2013
01/02/2013
01/03/2013
01/04/2013
01/05/2013
01/06/2013
01/07/2013
01/08/2013
01/09/2013
01/10/2013
01/11/2013
01/12/2013
Date

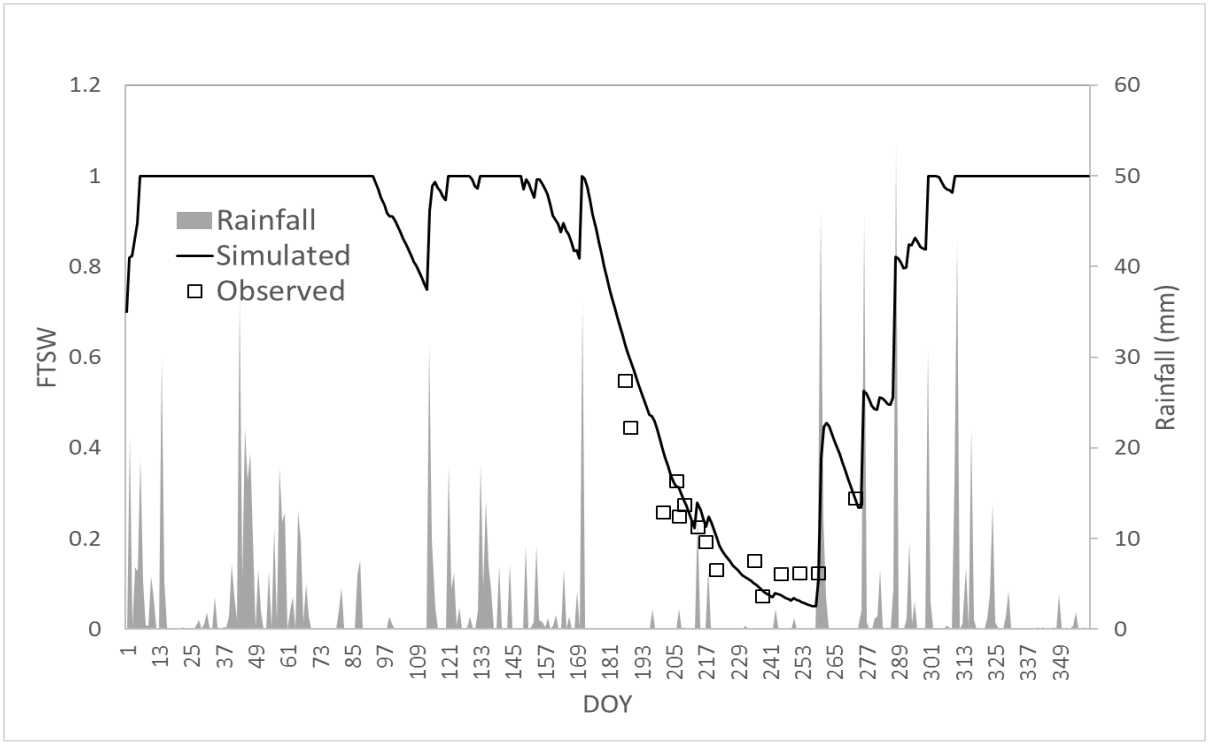
Rainfall
Simulated
Observed
FTSW
Rainfall (mm)
DOY

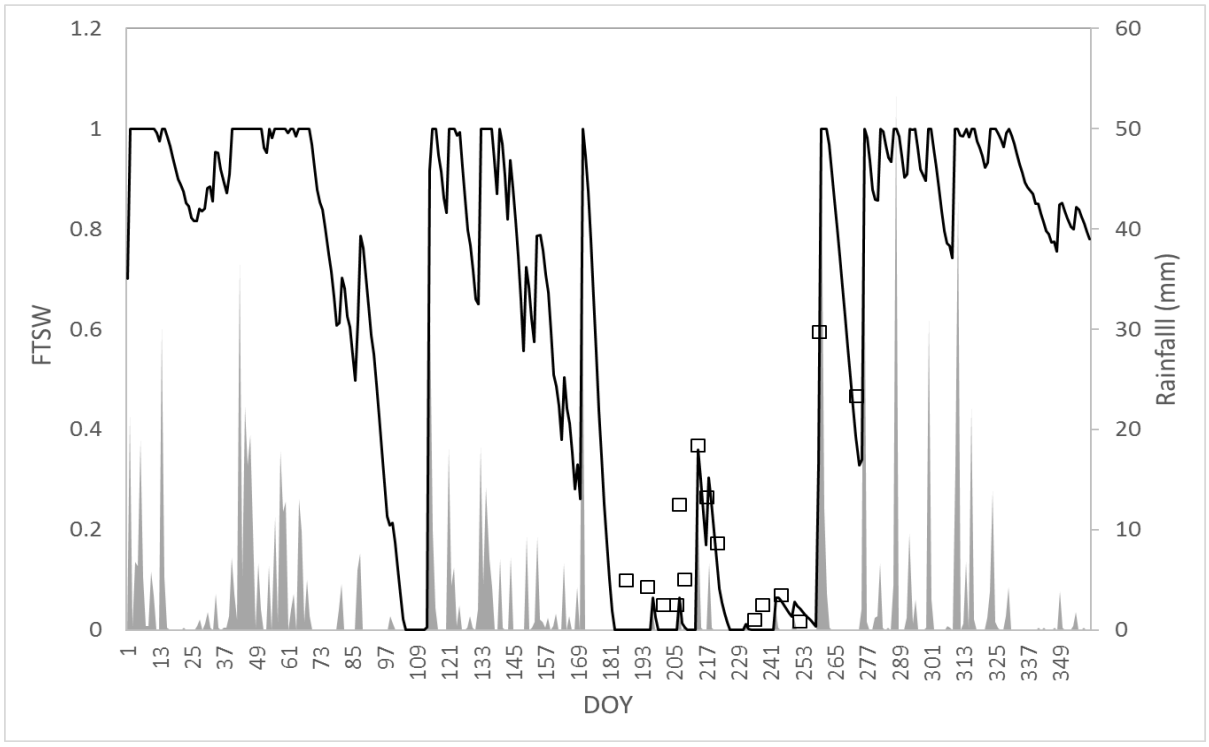
FTSW
Rainfalll (mm)
DOY

Figure 6

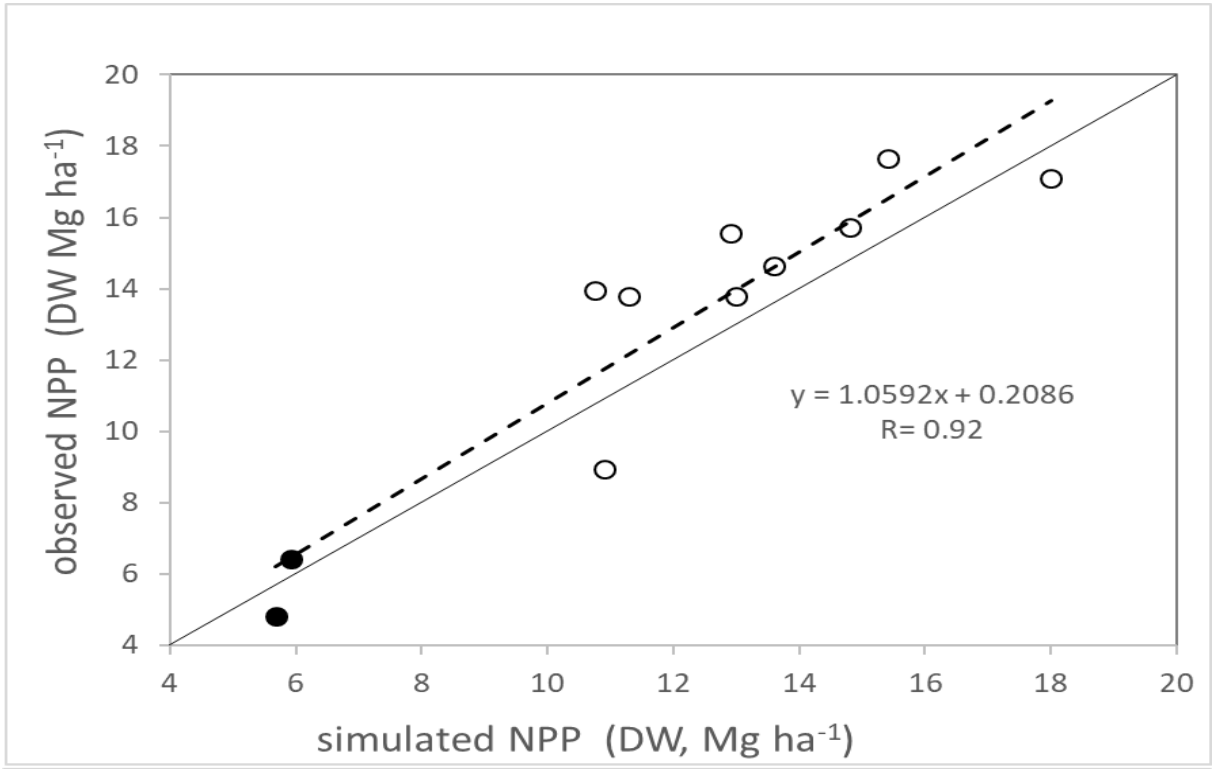

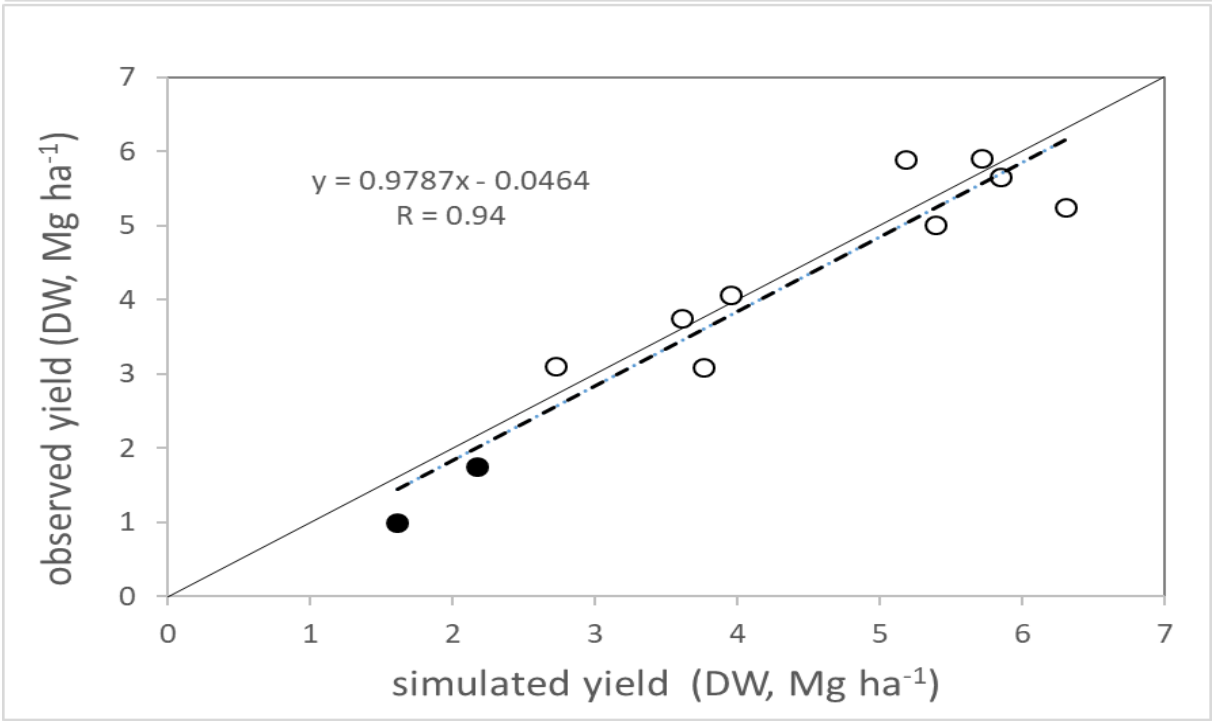

767

768 Figure 7

769

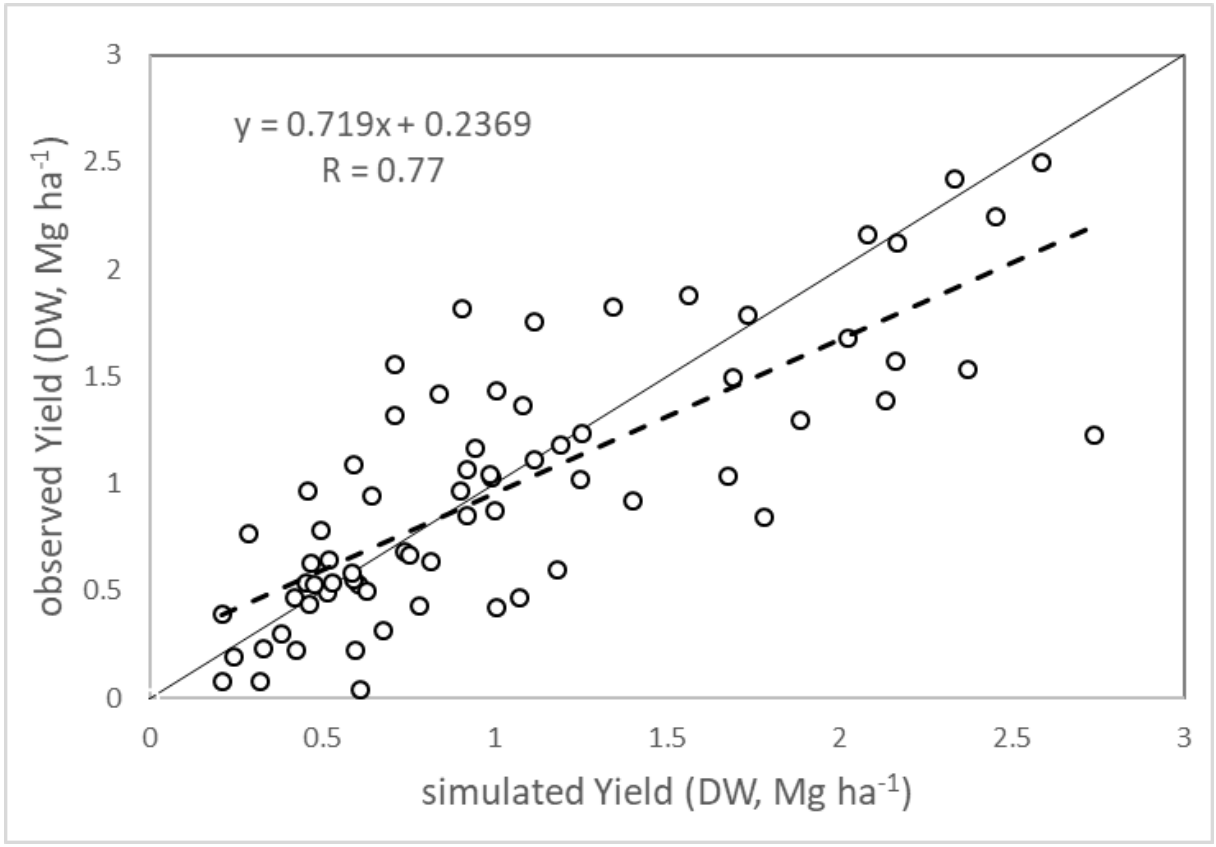

770

771 Figure 8

772

773

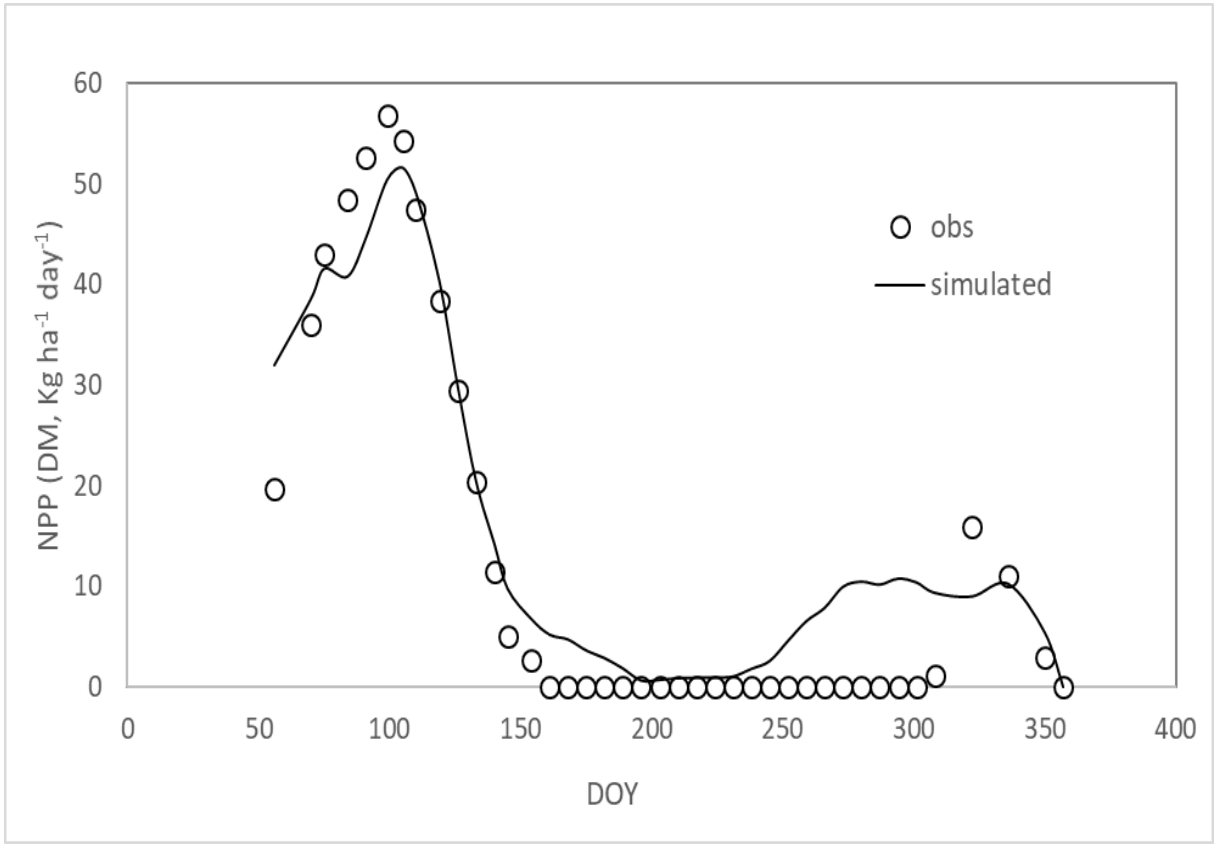

774

775 Figure 9

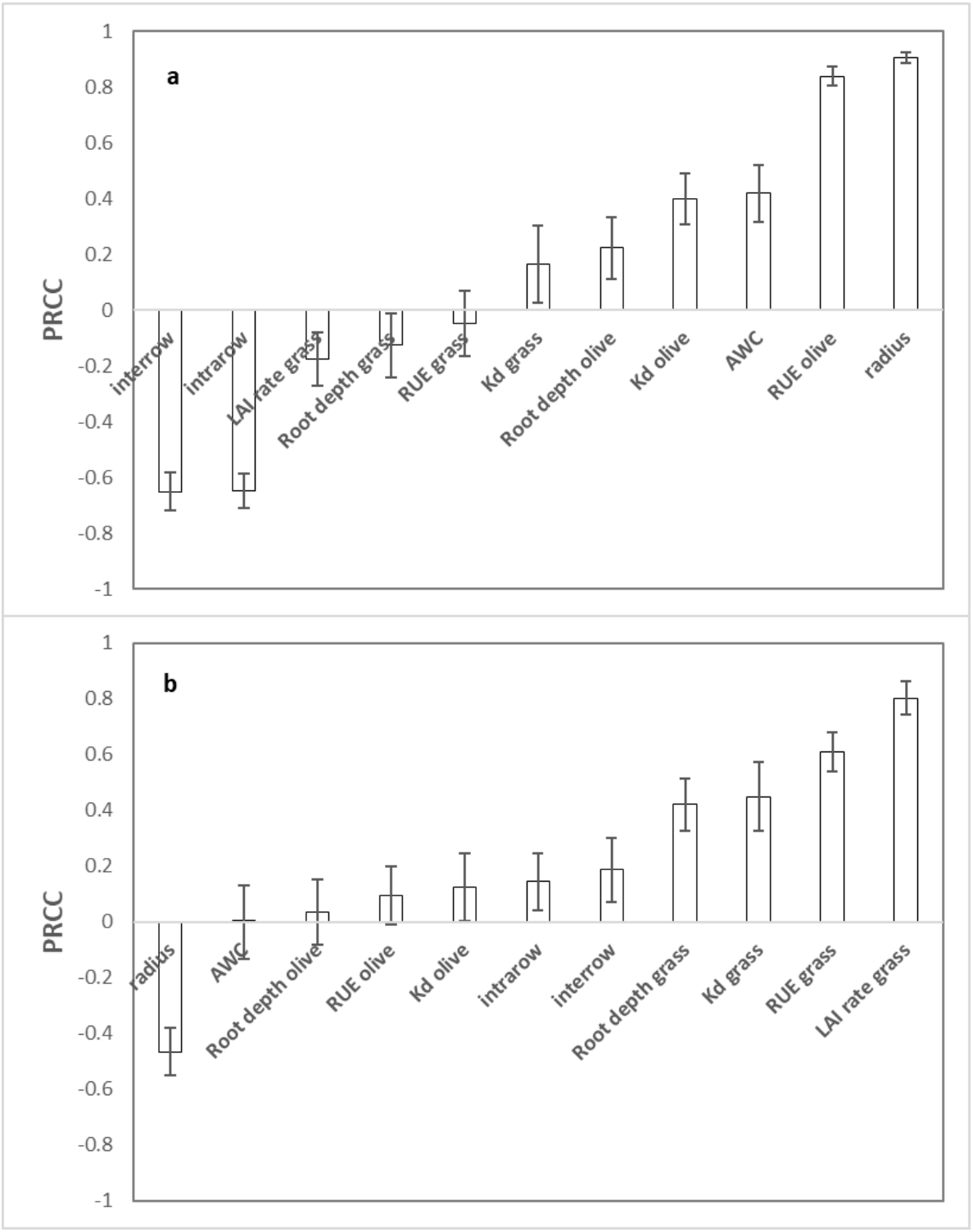

776

777 Figure 10.

References

Abdel-Razik, M., 1989. A model of the productivity of olive trees under optimal water and nutrient supply in desert conditions. Ecol. Model. 45 (3), 179–204.

Amir, J. Sinclair, T.R., 1991. A model of water limitation on spring wheat growth and yield. Field Crop Res. 28 (1-2), 59–69.

Argenti, G., 1994. Studio della possibilità di impiego del trifoglio sotterraneo in consociazione. PhD dissertation, University of Florence, 91p.

Argenti, G., Bottai, L., Chiesi, M., Maselli, F., Staglianò, N., Targetti, S., 2011. Analisi e valutazione di pascoli montani attraverso l'integrazione di dati multispettrali e ausiliari. Ital J Remote Sens. 43, 45-57.

Argenti, G., Cervasio, F., Ponzetta, M., 2012. Control of bracken (Pteridium aquilinum) and feeding preferences in pastures grazed by wild ungulates in an area of the Northern Apennines (Italy). Ital. J. Anim. Sci. 11 (4), 336-341.

Baldocchi, D., Valentini, R., Running, S., 1996. Strategies for measuring and modeling carbon dioxide and water vapour fluxes over terrestrial ecosystem. Glob. Change Biol. 2 (3), 159-168.

Battista, P., Chiesi, M., Rapi B., Romani, M., Cantini, C., Giovannelli, A., Cocozza C., Tognetti, R., Maselli, F. (2016). Integration of Ground and Multi-Resolution Satellite Data for Predicting the Water Balance of a Mediterranean Two-Layer Agro-Ecosystem. Remote Sens. 8(9):731.

Bélanger, G., Gastal, F., Lemaire, G., 1992. Growth of a tall fescue sward fertilized with different rates of nitrogen. Crop Sci. 32 (6), 1371-1376.

Bindi, M., Bellesi, S., Orlandini, S., Fibbi, L., Moriondo, M., Sinclair, T., 2005. Influence of water deficit stress on leaf area development and transpiration of Sangiovese grapevines grown in pots. Am. J. Enol. Viticult. 56 (1), 68-72.

Bindi, M., Miglietta, F., Gozzini, B., Orlandini, S., Seghi, L., 1997. A simple model for simulation of growth and development in grapevine (Vitis vinifera L.). II. Model validation. Vitis 36, 73-76.

804 Bongi, G., Long, S.P., 1987. Light dependent damage to photosynthesis in olive trees during chilling
805 and high temperatures stress. Plant Cell Environment 14, 127-132, http://dx.doi:10.1111/1365-
806 3040.ep11602267
807 Brilli, L, Gioli, B., Toscano, P., Moriondo, M., Zaldei, A., Cantini, C., Ferrise, R., Bindi, M., 2016.
808 Rainfall regimes control C-exchange of Mediterranean Olive orchard. Agr. Ecosys. Env. 233,
809 147-157.
810 Brilli, L., Chiesi, M., Maselli, F., Moriondo, M., Gioli, B., Toscano, P., Zaldei, A., Bindi, M., 2013.
811 Simulation of olive grove gross primary production by the combination of ground and multi-
812 sensor satellite data. Int. J. Appl. Earth Obs. Geoinf. 23, 29-36
813 Brilli, L., et al., 2017. Review and analysis of strengths and weaknesses of agro-ecosystem models in
814 representing C and N fluxes. Sci. Total Environ. 598, 445-470.
815 Brilli, L., Ferrise, R., Lugato, E., Moriondo, M., Bindi, M. 2014. Using mitigation and adaptation
816 strategies to optimize crop yield and greenhouse gas emissions. In: Sustainable agroecosystems
817 in climate change mitigation (Maren Oelbermann, editor), Wageningen Academic Publisher,
818 Netherland, ISBN: 978-90-8686-235-1.
819 Jones, C.A., Kiniry J.R., 1986. CERES-Maize: a Simulation Model of Maize Growth and
820 Development, Texas A&M University Press, College Station, TX, USA (1986)
821 Caffarra, A., Eccel, E., 2010. Increasing the robustness of phenological models for Vitis vinifera cv.
822 Chardonnay. Int. J. Biometeorol. 54 (3), 255–267.
823 Calanca, P., Deléglise, C., Martin, R., Carrère, P., Mosimann, E., 2016. Testing the ability of a simple
824 grassland model to simulate the seasonal effects of drought on herbage growth. Field Crop
825 Res. 187, 12-23.
826 Carr, M.K.V., 2014. Advances in Irrigation Agronomy: Fruit Crops. Cambridge University Press,
827 New York 350 pp. ISBN: 9781107037359

828 Caruso, G., Rapoport, H. F., Gucci, R., 2013. Long-term evaluation of yield components of young
829 olive trees during the onset of fruit production under different irrigation regimes. Irrigation
830 Sci. 31 (1), 37-47.
831 Caruso, G., Tozzini, L., Rallo, G., Primicerio, J., Moriondo, M., Palai, G., Gucci, R., 2017. Estimating
832 biophysical and geometrical parameters of grapevine canopies ('Sangiovese') by an unmanned
833 aerial vehicle (UAV) and VIS-NIR cameras. Vitis 56 (2), 63-70.
834 Celette, F., Ripoche, A., Gary, C., 2010. WaLIS—A simple model to simulate water partitioning in
835 a crop association: The example of an intercropped vineyard. Agric. Wat. Manage. 97 (11),
836 1749–1759.[HC3]
837 Challinor, A.J., Wheeler, T.R., Craufurd, P.Q., Slingo, J.M., 2005. Simulation of the impact of high
838 temperature stress on annual crop yields. Agric. For. Meteorol. 135 (1), 180-189.
839 Challinor, A.J., Wheeler, T.R., Craufurd, P.Q., Slingo, J.M., Grimes, D.I.F., 2004. Design and
840 optimization of a large-area process-based model for annual crops, Agric. For. Meteorol. 124
841 (1), 99-120.
842 Chartzoulakis, K., Patakas, A., Bosabalidis, A.M., 1999. Changes in water relations, photosynthesis
843 and leaf anatomy induced by intermittent drought in two olive cultivars. Environ. Exp. Bot. 42
844 (2), 113-120.
845 chilling temperature regimes. J. Amer. Soc. Hort. Sci. 100, 670-674
846 Chollet, S., Rambal, S., Fayolle, A., Hubert, D., Foulqui, D. Garnier, E. 2014. Combined effects of
847 climate, resource availability, and plant traits on biomass produced in a Mediterranean
848 rangeland. Ecology 95 (3), 737-748.
849 Chuine, I., 2000. A unified model for budburst of trees. J. Theor. Biol. 207 (3), 337-347.
850 Clayden, J., 2014. General-Purpose Optimisation With the Self-Organising Migrating Algorithm.
851 Cobos, D., 2015. Measurement volume of Decagon volumetric water content sensors. In Application
852 Note Decagon Devices, Decagon Devices Inc., Pullman, WA, USA, pp. 1- 4.

853 Cocozza, C., Marino, G., Giovannelli, A., Cantini, C., Centritto, M., Tognetti R., 2015. Simultaneous
854 measurements of stem radius variation and sap flux density reveal synchronization of water
855 storage and transpiration dynamics in olive trees. Ecohydrology 8 (1), 33-45.
856 Cola, G., Mariani, L., Salinari, F., Civardi, S., Bernizzoni, F., Gatti, M., Poni, S., 2014. Description
857 and testing of a weather-based model for predicting phenology, canopy development and
858 source–sink balance in Vitis vinifera L. cv. Barbera. Agric. For. Meteorol. 184, 117-136.
859 Congreves, K.A., Grant, B.B., Dutta, B., Smith, W.N., Chantigny, M.H., Rochette, P., Desjardins,
860 R.L., 2016. Predicting ammonia volatilization after field application of swine slurry: DNDC
861 model development. Agric Ecosyst Environ. 219, 179-189.
862 Corrall, A.J., Fenlon, J. S., 1978. A comparative method for describing the seasonal distribution of
863 production from grasses. J. Agric. Sci. 91 (1), 61-67.
864 Confalonieri, R., Bellocchi, G., Bregaglio, S., Donatelli, M., Acutis, M., 2010. Comparison of
865 sensitivity analysis techniques: a case study with the rice model WARM. Ecological Modelling
866 221 (16), 1897–1906.
867 d'Andria, R., Lavini, A., Morelli, G., Sebastiani, L., Tognetti, R. 2009. Physiological and productive
868 responses of *Olea europaea* L. cultivars Frantoio and Leccino to a regulated deficit irrigation
869 regime. Plant Biosyst. 143, 222-231.
870 De Melo-Abreu, J.P., Barranco, D., Cordeiro, A.M., Tous, J., Rogado, B.M., Villalobos, F.J., 2004.
871 Modelling olive flowering date using chilling for dormancy release and thermal time. Agric.
872 For. Meteorol. 125 (1), 117-127.
873 DOI: 10.17660/ActaHortic.2017.1160.33 https://doi.org/10.17660/ActaHortic.2017.1160.33
874 D'Onofrio, D., Baudena, M., D'Andrea, F., Rietkerk, M., Provenzale, A. 2015. Tree- grass
875 competition for soil water in arid and semiarid savannas: The role of rainfall
876 intermittency. Water Resour. Res. 51 (1), 169-181.

877 Duru M., Ducrocq H., Tirilly V., 1995. Modeling growth of cocksfoot (Dactylis glomerata L.) and
878 tall fescue (Festuca arundinacea shreb.) at the end of spring in relation to herbage nitrogen
879 status. J. Plant Nutr. 18 (10), 2033–2047.
880 Fernández, J.E., Diaz-Espejo, A., d'Andria, R., Sebastiani, L., Tognetti R. 2008. Potential and
881 limitations of improving olive orchard design and management through modelling. Plant
882 Biosyst. 142, 130–137.
883 Ferrise, R., Moriondo, M., Trombi, G., Miglietta, F., Bindi, M., 2013. Climate change impacts on
884 typical Mediterranean crops and evaluation of adaptation strategies to cope with. In Regional
885 Assessment of Climate Change in the Mediterranean (pp. 49-70). Springer Netherlands.
886 Fitton, N., Datta, A., Hastings, A., Kuhnert, M., Topp, C.F.E., Cloy, J.M., Rees, R.M., Cardenas,
887 L.M., Williams, R.J., Smith, K., Chadwick, D., Smith, P., 2014b. The challenge of modelling
888 nitrogen management at the field scale: simulation and sensitivity analysis of N2O fluxes across
889 nine experimental sites using DailyDayCent. Environ Res Lett. 9, 095003.
890 Fitton, N., Datta, A., Smith, K., Williams, J.R., Hastings, A., Kuhnert, M., Topp, C.F.E., Smith, P.,
891 2014a. Assessing the sensitivity of modelled estimates of N2O emissions and yield to input
892 uncertainty at a UK cropland experimental site using the DailyDayCent model. Nutr. Cycl.
893 Agroecosys. 99 (1-3), 119-133.
894 Fleskens, L., Duarte, F., Eicher, I., 2008. A conceptual framework for the assessment of multiple
895 functions of agro-ecosystems: A case study of Trás-os-Montes olive groves. J. Rural Stud. 25
896 (1), 141-155.
897 Foken, T., Gockede, M., Mauder, M., Mahrt, L., Amiro, B.D., Munger, J.W., 2004. Postfield data
898 quality control. In: Lee, X. (Ed.), Handbook of Micrometeorology: A Guide for Surface Flux
899 Measurements. Kluwer Academic Publishers, Dordrecht, pp. 81–108.
900 Galán, C., Cariñanos, P., García-Mazo, H., Alcázar, P., Domínguez-Vilches, E., 2001. Model for
901 forecasting Olea europaea L. airborne pollen in South-West Andalusia, Spain. Int. J.
902 Biometeorol. 45 (2), 59-63.

903 Gardin, L., Vinci A., 2006. Carta dei suoli della Regione Toscana in scala-1:250.000.
904 http://sit.lamma.rete.toscana.it/websuoli/.
905 Ghamkhar, K., Nichols, P.G.H., Erskine, W., Snowball, R., Murillo, M., Appels R., Ryan M.H., 2015.
906 Hotspots and gaps in the world collection of subterranean clover (Trifolium subterraneum L.).
907 J. Agric. Sci. 153 (6), 1069-1083.
908 Giltrap, D.L., Vogeler, I., Cichota, R., Luo, J., van der Weerden, T.J., de Klein, C.A.M., 2015.
909 Comparison between APSIM and NZ-DNDC models when describing N-dynamics under urine
910 patches. New Zeal. J. Agr. Res. 58 (2), 131-155.
911 Granier, A., 1985. A new method of sap flow measurement in tree stems. Ann. For. Sci. 42, 193-200.
912 Graniti, A., Faedda R., Cacciola S.O., Magnano di San Lio G., 2011. Olive diseases in a changing
913 ecosystem. In: Schena L., Agosteo G.E., Cacciola S.O. (eds). Olive Diseases and Disorders, pp.
914 403-433. Transworld Research Newtwork, Trivandrum, Kerala, India.
915 Gucci, R., et al., 2012. Changes of soil properties and tree performance induced by soil management
916 in a high-density olive orchard. Eur. J Agron. 41, 18-27.
917 Hartmann, H.T. and J.W. Whisler. 1975. Flower production in olive as influenced by various
918 Hunter, A.F., Lechowicz, M.J., 1992. Predicting the Timing of Budburst in Temperate Trees. J. Appl.
919 Ecol. 29, 597–604.
920 Iraldo, F., Testa, F., Bartolozzi, I., 2013. An application of Life Cycle Assessment (LCA) as a green
921 marketing tool for agricultural products: the case of extra-virgin olive oil in Val di Cornia, Italy,
922 J. Environ. Plann. Man. 57 (1), 78-103.
923 Koukoura, Z. 2007. Natural Grasslands-a Case Study in Greece. In: Marschner P., Rengel Z. (eds)
924 Nutrient Cycling in Terrestrial Ecosystems. Soil Biology, vol 10, pp. 257-269. Springer, Berlin,
925 Heidelberg.
926 Lavee, S., 2007. Biennial bearing in olive (Olea europaea). Annales Ser. His. Nat. 17, 101-112.

927 Li, H., Qiu, J., Wang, L., Tang, H., Li, C., Van Ranst, E., 2010. Modelling impacts of alternative
928 farming management practices on greenhouse gas emissions from a winter wheat–maize
929 rotation system in China. Agric. Ecosyst. Environ. 135 (1), 24-33.
930 López-Bernal, A., Villalobos, F.J., García-Tejera, O., Testi, L. and Orgaz, F. (2017). Do olive
931 vegetative buds undergo a real dormant state in winter?. Acta Hortic. 1160, 227-230
932 Loumou, A., Giourga, C., 2003. Olive groves: the life and identity of the Mediterranean. Agric.
933 Human Values 20 (1), 87–95.
934 Maiorano, A., et al., 2017. Crop model improvement reduces the uncertainty of the response to
935 temperature of multi-model ensembles. Field Crop Res. 202, 5-20.
936 Mancuso, S., Pasquali, G., Fiorino, P., 2002. Phenology modelling and forecasting in olive (Olea
937 europaea L .) using artificial neural networks. Adv. Hortic. Sci. 16, 155-164.
938 Marino, G., Pallozzi, E., Cocozza, C., Tognetti, R., Giovannelli, A., Cantini, C., Centritto M., 2014.
939 Assessing gas exchange, sap flow and water relations using tree canopy spectral reflectance
940 indices in irrigated and rainfed Olea europaea L.. Environ. Exp. Bot. 99, 43-52.
941 Mariscal, M.J., Orgaz, F., Villalobos, F.J., 2000. Radiation-use efficiency and dry matter partitioning
942 of a young olive (Olea europaea) orchard. Tree Physiol. 20 (1), 65-72.
943 Marra, F.P., 2009. Ambiente di Coltivazione. In M. Pisante, P. Inglese, & G. Lercker (Eds.), L'Ulivo
944 e l'Olio (pp. 350-357). Citta di Castello (PG) : ART S.p.A. Ed. Script, Bologna, Italy.
945 Maselli, F., Chiesi, M., Brilli, L., Moriondo, M., 2012. Simulation of olive fruit yield in Tuscany
946 through the integration of remote sensing and ground data. Ecol. Model. 244, 1-12.
947 Matese, A., Alberti, G., Gioli, B., Toscano, P., Vaccari, F.P., Zaldei, A., 2008. Compact eddy: a
948 compact, low consumption remotely controlled eddy covariance logging system. Comput.
949 Electron. Agric. 64 (2), 343–346.
950 Matese, A., Di Gennaro, S.F., Berton, A., 2017. Assessment of a canopy height model (CHM) in a
951 vineyard using UAV-based multispectral imaging. Int. J. Remote Sens. 38 (8-10), 2150-2160.

952 Moncrieff, J., Massheder, J.M., de Bruin, H., Elbers, J., Friborg, T., Heusinkveld, B., Kabat, P., Scott,
953 S., Soegaard, H., Verhoef, A., 1997. A system to measure surface fluxes of momentum, sensible
954 heat, water vapour and carbon dioxide. J. Hydrol. 188, 589–611.
955 Monteith, J. L., 1996. The quest for balance in crop modeling. Agronomy Journal 88(5), 695-697.
956 Morales, A., Leffelaar, P.A., Testi, L., Orgaz, F., Villalobos, F.J., 2016. A dynamic model of potential
957 growth of olive (Olea europaea L.) orchards. Eur. J. Agron. 74, 93-102.
958 Moreno F, Fernandez E, Clothier BE and Green SR (1996). Transpiration and root water uptake by
959 olive trees. Plant Soil 184 (1), 85–96.
960 Moriana, A., Orgaz, F., Pastor, M., Fereres, E., 2003. Yield responses of a mature olive orchard to
961 water deficits. Journal of the American Society for Horticultural Science, 128(3), 425-431.
962 Moriondo, M., Ferrise, R., Trombi, G., Brilli, L., Dibari, C., Bindi, M., 2015. Modelling olive trees
963 and grapevines in a changing climate. Environ. Model. Softw. 72, 387-401.
964 Moriondo, M., Argenti, G., Ferrise, R., Dibari, C., Trombi, G., Bindi, M., 2016. Heat stress and crop
965 yields in the Mediterranean basin: impact on expected insurance payouts. Reg. Environ.
966 Change 16 (7), 1877-1890.
967 Moriondo, M., Giannakopoulos, C., Bindi, M., 2011. Climate change impact assessment: the role of
968 climate extremes in crop yield simulation. Clim. Change 104 (3-4), 679-701.
969 Moriondo, M., Orlandini, S., De Nuntiis, P., Mandrioli, P., 2001. Effect of agrometeorological
970 parameters on the phenology of pollen emission and production of olive trees (Olea europea
971 L.). Aerobiologia 17 (3), 225-232.
972 Moriondo, M., Stefanini, F. M., Bindi, M., 2008. Reproduction of olive tree habitat suitability for
973 global change impact assessment. Ecol. Model. 218 (1), 95-109.
974 Moriondo, M., Trombi, G., Ferrise, R., Brandani, G., Dibari, C., Ammann, C.M., Mariotti Lippi, M.,
975 Bindi, M. 2013. Olive trees as bio- indicators of climate evolution in the Mediterranean
976 Basin. Glob. Ecol. Biogeogr. 22 (7), 818-833.

977 Nardino, M., Pernice, F., Rossi, F., Georgiadis, T., Facini, O., Motisi, A., Drago, A., 2013. Annual
978 and monthly carbon balance in an intensively managed Mediterranean olive
979 orchard. Photosynthetica 51 (1), 63-74.
980 Nieto, O.M., Castro, J., Fernández, E., Smith, P., 2010. Simulation of soil organic carbon stocks in a
981 Mediterranean olive grove under different soil-management systems using the RothC model,
982 Soil Use Manage. 26 (2), 118-125.
983 Noirot-Cosson, P.E., Vaudour, E., Gilliot, J.M., Gabrielle, B., Houot, S., 2016. Modelling the long-
984 term effect of urban waste compost applications on carbon and nitrogen dynamics in temperate
985 cropland. Soil Biol. Biochem. 94, 138-153.
986 Orlandi, F., Garcia-Mozo, H., Ezquerra, L.V., Romano, B., Dominguez, E., Galan, C., Fornaciari,
987 M., 2004. Phenological olive chilling requirements in Umbria (Italy) and Andalusia (Spain).
988 Plant Biosyst. 138 (2), 111-116.
989 Palese, A.M., Pergola, M., Favia, M., Xiloyannis, C., Celano, G., 2013. A sustainable model for the
990 management of olive orchards located in semi-arid marginal areas: Some remarks and
991 indications for policy makers. Environ. Sci. Policy 27, 81-90.
992 Panagopoulos, T, Neves, M.A., 2017. Vegetation Cover for Sustainable Olive Grove Management.
993 Proc. of the 3rd IASME/WSEAS Int. Conf. on Energy, Environment, Ecosystems and
994 Sustainable Development, Agios Nikolaos, Greece, July 24-26, 2007, pp. 71-74.
995 Ponti, L., Gutierrez, A. P., Ruti, P. M., Dell'Aquila, A. 2014. Fine-scale ecological and economic
996 assessment of climate change on olive in the Mediterranean Basin reveals winners and
997 losers. PNAS 111 (15), 5598-5603.
998 R Core Team, 2015. R: A language and environment for statistical computing.
999 Rallo, G., Provenzano, G., 2013. Modelling eco-physiological response of table olive trees (Olea
1000 europaea L.) to soil water deficit conditions. Agr. Water Manage. 120, 79-88.
1001 Rapetti, F., Vittorini, S., 1995. Carta climatica della Toscana. Pacini Editore, Pisa (Italy).

Rapoport, H. F., Hammami, S. B., Martins, P., Pérez-Priego, O., & Orgaz, F. (2012). Influence of water deficits at different times during olive tree inflorescence and flower development. *Environmental and Experimental Botany*, *77*, 227-233.

Rapoport, H.F., Pérez-Priego, O., Orgaz, F., Martins, P., 2011. Water deficit effects during olive tree inflorescence and flower development. Acta Hort. 888, 157-162.

Rapoport, H.F., 2012. The reproductive biology of the olive tree and its relationship to extreme environmental conditions. In *VII International Symposium on Olive Growing 1057* (pp. 41-50).

Reichstein, M., et al., 2005. On the separation of net ecosystem exchange into assimilation and ecosystem respiration: review and improved algorithm. Global Change Biol. 11 (9), 1-16.

Richardson, E.A., Seeley, S.D., Walker, D.R., 1974. A model for estimating the completion of rest for Redhaven and Elberta peach trees. HortSci.ence 9, 331–332.

Saxton, K. E., Rawls, W., Romberger, J. S., Papendick, R. I. 1986. Estimating generalized soil-water characteristics from texture 1. Soil Science Society of America Journal, 50(4), 1031-1036.

Scandellari, F., Caruso, G., Liguori, G., Meggio, F., Palese, A.M., Zanotelli, D., Celano, G., Gucci, R., Inglese, P., Pitacco, A., Tagliavini, M. (2016). A survey of carbon sequestration potential of orchards and vineyards in Italy. Eur.J.Hortic.Sci. 81(2), 106-114.

Schoppach, R., Sadok, W., 2012. Differential sensitivities of transpiration to evaporative demand and soil water deficit among wheat elite cultivars indicate different strategies for drought tolerance. Environ Exp. Bot. 84, 1-10.

Shaltout, A.D., Unrath, C.R., 1983. Rest completion prediction model for Starkrimson delicious apples. J. Am. Soc. Hort. Sci. 108 (6), 957–961.

Sinclair, T.R., 1986. Water and nitrogen limitations in soybean grain production. I. Model development. Field Crops Res. 15 (2), 125-141.

Sinclair, T.R., Hammond, L.C., Harrison, J., 1998. Extractable soil water and transpiration of soybean on sandy soils. Agron. J. 90 (3), 363-368.

1027 Sinclair, T.R., Seligman, N.A., 2000. Criteria for publishing papers on crop modeling. Field Crop
1028 Res. 68 (3), 165-172.
1029 Sinclair, T.R., Tanner, C.B., Bennett, J.M., 1984. Water-use efficiency in crop
1030 production. Bioscience 34 (1), 36-40.
1031 Sofo, A., Manfreda, S., Fiorentino, M., Dichio, B., Xiloyannis, C., 2008. The olive tree: a paradigm
1032 for drought tolerance in Mediterranean climates. Hydrol. Earth Syst. Sci. Discuss. 12 (1), 293-
1033 301.
1034 Sofo, A., Nuzzo, V., Palese, A. M., Xiloyannis, C., Celano, G., Zukowskyj, P., Dichio, B., 2005. Net
1035 CO 2 storage in Mediterranean olive and peach orchards. Sci. Hortic. 107 (1), 17-24.
1036 Soltani, A. Sinclair, T.R., 2011. A simple model for chickpea development, growth and yield. Field
1037 Crop Res. 124 (2), 252-260.
1038 Soltani, A., Sinclair T. R., 2012. Modeling physiology of crop development, growth and yield. CABI,
1039 2012.
1040 Spelman, D.; Kinzli, K.; Kunberger, T., 2013. Calibration of the 10HS soil moisture sensor for
1041 southwest Florida agricultural soils. J. Irrig. Drain. Eng. 139 (12), 965–971.
1042 Tanner, C.B., and T.R. Sinclair., 1983. Efficient water use in crop production: research or research.
1043 Pages 1-28 in H. Taylor et al. eds. Limitations to Efficient Water Use in Crop Production.
1044 American Society Agronomy, Madison.
1045 Testi, L., Villalobos, F. J., Orgaz, F., Fereres, E., 2006. Water requirements of olive orchards: I
1046 simulation of daily evapotranspiration for scenario analysis. *Irrigation Science*, *24*(2), 69-76.
1047 Thornthwaite, C.W., 1948. An approach toward a rational classification of climate. Geogr. Rev. 38
1048 (1), 55–94.
1049 Tognetti, R., Giovannelli, A., Lavini, A., Morelli, G., Fragnito, F. d'Andria, R. 2009. Assessing
1050 environmental controls over conductance through the soil-plant-atmosphere continuum in an
1051 experimental olive tree plantation of southern Italy. Agric. For. Meteorol. 149 (8), 1229-1243.

1052 Villalobos, F.J., Testi, L., Hidalgo, J., Pastor, M., Orgaz, F. 2006. Modelling potential growth and
1053 yield of olive (Olea europaea L.) canopies. Eur. J. Agron. 24 (4), 296-303.
1054 Viola, F., Noto, L.V., Cannarozzo, M., La Loggia, G., Porporato, A., 2012. Olive yield as a function
1055 of soil moisture dynamics. Ecohydrology 5 (1), 99-107.
1056 Vossen, P., 2007. Olive oil: History, production, and characteristics of the world's classic oils.
1057 Hortscience 42 (5), 1093-1100.
1058 Xiloyannis, C., Dichio, B., Nuzzo, V., Celano, G., 1999. Defense strategies of olive against water
1059 stress. Acta Hortic. 474, 423-426.
1060 Zarco-Tejada, P.J., Diaz-Varela, R., Angileri, V., Loudjani, P., 2014. Tree height quantification using
1061 very high resolution imagery acquired from an unmanned aerial vehicle (UAV) and automatic
1062 3D photo-reconstruction methods. Eur. J. Agron. 55, 89-99.
1063
1064
1065